MODELING AND OBSERVATIONAL STUDIES OF SEA ICE - MIXED LAYER INTERACTIONS ON THE WEST ANTARCTIC PENINSULA CONTINENTAL SHELF

by

David Allen Smith
B.S. June 1990, West Virginia University

A Dissertation Submitted to the Faculty of
Old Dominion University in Partial Fulfillment of the
Requirements for the Degree of

DOCTOR OF PHILOSOPHY

OCEANOGRAPHY

OLD DOMINION UNIVERSITY
December 1999

Approved by:

John M Klinck
J. M. Klinck (Director of Advisory Committee)

Eileen E. Hofmann
E. E. Hofmann (Member)

Larry P. Atkinson
L. P. Atkinson (Member)

Douglas G Martinson
D. Martinson (Member)

ABSTRACT

MODELING AND OBSERVATIONAL STUDIES OF SEA ICE - MIXED LAYER INTERACTIONS ON THE WEST ANTARCTIC PENINSULA CONTINENTAL SHELF

David Allen Smith
Old Dominion University, 1999
Director: Dr. J. M. Klinck

Meteorological and hydrographic observations collected between January and August of 1993 are used to characterize the hydrographic structure, heat content, heat exchange at the air/ice/sea interface and to force numerical models for the continental shelf waters to the west of the Antarctic Peninsula.

Individual components for the 1993 heat budget are quantified and ranked indicating that incoming short wave radiation (Q_{sw}), with values in excess of 150 to 200 W m^{-2}, dominate the overall summer budget. Conversely, the winter budget is dominated by sensible heat losses which typically on the order of 50 W m^{-2} with episodic losses exceeding values of 150 W m^{-2}. These episodic losses coincide with periods of cold atmospheric temperatures (T_{air} < -15 °C) and are on the same time scales as those associated with the passage of synoptic low pressure systems through Drake Passage.

A vertical time-dependent thermodynamic ice-ocean model is developed and forced with 1993 heat fluxes to further investigate the vertical transfer of heat through Antarctic Surface Water (AASW) and to characterize the time dependent hydrographic structure of the mixed layer. The timing of the simulated ice cycle was consistent with the timing of a satellite derived ice cycle. The simulations indicate that a heat loss of 10 to 20 W m^{-2} from AASW to the ice persist through the year and that a balance between this heat loss and heat fluxes at the ice/ocean interface control overall ice growth. A persistent resupply of heat through the pycnocline to the base of AASW on the order of 10 to 20 W m^{-2} is simulated and is primarily

driven by double diffusion. The differential vertical transfer of heat and salt resulting from double diffusion is shown to be important to the hydrographic structure of AASW.

The numerical simulations and the heat flux calculations based on 1993 hydrographic and meteorological data indicate that vertical processes are important to the hydrographic structure of the mixed layer along the west Antarctic Peninsula. Horizontal processes, such as advection, such as advection are not necessary to close regional heat budgets.

Copyright, 1999, by David Allen Smith, All Rights Reserved.

This dissertation is dedicated to my family.

ACKNOWLEDGMENTS

This work was supported by the National Science Foundation Office of Polar Science under the grant number DPP-900-11927 and OPP-96-32763. Computer support and facilities were provided by the Center for Coastal Physical Oceanograhy.

I sincerely thank Drs. John Klinck and Eileen Hofmann for their support throughout my tenure as a student. I am also thankful to the members of the faculty and staff who had an interest in my education at the Center for Coastal Physical Oceanography. I am especially thankful to the members of my dissertation committee Drs. Larry Atkinson and Douglass Martinson for their guidance throughout the project.

I am very fortunate to have shared my graduate experience with many students at the Center for Coastal Physical Oceanography. In particular I would like to thank former office mates Cathy Lascara and John Holdzkom. My graduate experience was greatly enriched by my professional and personal relationships with Cathy and John.

To my parents, David and Sandy, I am grateful for the advice, support and guidance that you gave me through the years. Finally I would like to thank my wife, Robin, and my two daughters Marianna and Alison. I can not imagine what my experience would have been like without your never ending love and support.

TABLE OF CONTENTS

TABLE OF CONTENTS (continued)

Page

TABLE OF CONTENTS (continued) Page

TABLE OF CONTENTS (continued)

LIST OF TABLES

Page

LIST OF FIGURES

Page

LIST OF FIGURES (continued) Page

LIST OF FIGURES (continued) Page

CHAPTER 1

INTRODUCTION

The waters to the west of the Antarctic Peninsula (WAP) (Figure 1) have long been recognized for their biological importance. Marr's [1962] interpretation of the 1934 *Discovery* data indicated that shelf waters to the west of Antarctic Peninsula are a region with abundant concentrations of Antarctic krill (*Euphausia superba*). The biological importance of the region has received extensive attention since Marr's [1962] original observation in such international programs as the First and Second International Biomass Experiments (FIBEX and SIBEX, respectively) [Gordon and Nowlin, 1978; Everson and Miller, 1994; Nowlin and Clifford, 1982; Sievers and Nowlin, 1984; Stein, 1983; Stein and Rakusa-Suszczewiski, 1983, 1984; and Stein, 1986, 1989] and German research efforts [Huntley et al., 1991; Niiler et al., 1991 and Stein, 1992].

In 1990, the National Science Foundation funded a Long-Term Ecological Research (LTER) site based at Palmer Station (i.e. Palmer LTER program), on Anvers Island (Figure 1), designed to study the ecology along the west Antarctic Peninsula shelf and its relation to the physical environment. The central hypothesis of the program is that many of the observed biological processes along the west Antarctic Peninsula shelf are related to the seasonal advance and retreat of the ice edge [Smith et al., 1995].

The waters to the west of the Antarctic Peninsula are characterized by a seasonal ice cover which cycles between nearly ice-free, summer conditions to full ice cover in the winter [Stammerjohn and Smith, 1996]. The maximum extent of the winter ice cover exhibits interannual variability characterized by years of high and low ice cover. The ice cycle is correlated with cold and warm winter atmospheric conditions

[1] The *Journal of Geophysical Research* was used as the journal model.

[Stammerjohn and Smith, 1996].

The primary objective of this research is to identify, quantify and rank the importance of physical processes which underlie the observed hydrographic structure and mixed layer dynamics within the continental shelf waters to the west of the Antarctic Peninsula. It is believed that key features in the mixed layer, which affect the region's biological processes, are determined by physical processes such as exchange of heat and salt at the air-ice-sea interface and across-shelf interactions with the Antarctic Circumpolar Current (ACC). It is also believed that the ocean may play an important feedback role in the complex atmosphere/ice cycle within the region. The approach taken to achieve this objective will involve the analysis of hydrographic and atmospheric data to form conceptual models of water mass interaction and surface heat flux exchanges. These conceptual models will then be extended into numerical studies.

The specific research questions addressed in this research are:

- Given the spatial and temporal variability of the water masses along the western Antarctic Peninsula shelf, what can be inferred about the underlying physics?

- What are the relative contributions of wind mixing, buoyancy forcing (i.e. ice related process and atmospheric fluxes), double diffusion and other vertical processes on the time evolution of the surface mixed layer?

- To what extent can vertical processes account for observed hydrographic structure, mixed-layer dynamics and temporal sea ice distributions? Are horizontal exchanges necessary to balance the vertical processes?

In recognition of the limited historical data coverage along the west Antarctic Peninsula [Hofmann et al., 1996], the Palmer LTER program includes a component

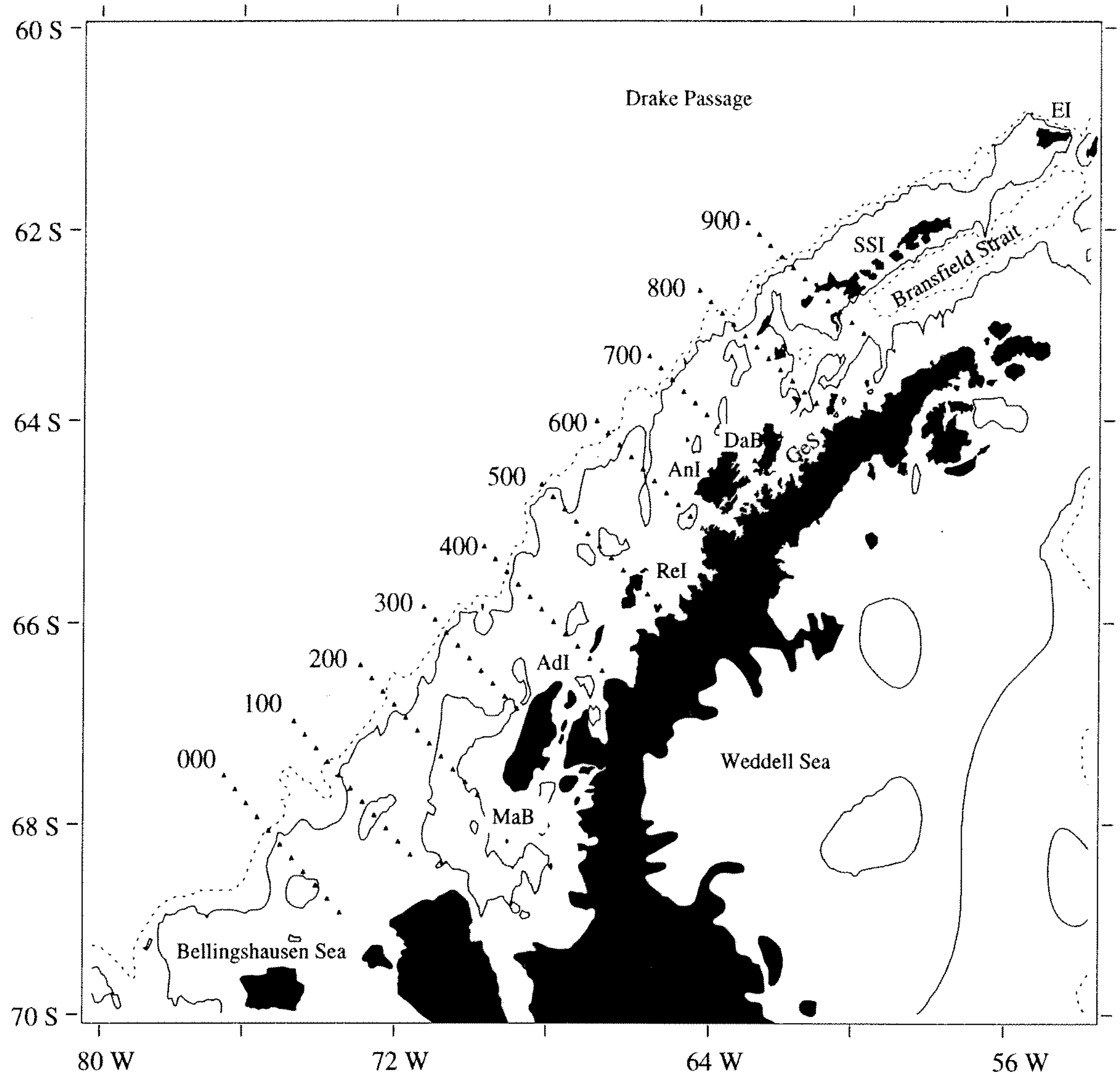

Figure 1. Palmer LTER study region along the west Antarctic Peninsula continental shelf. The across-shelf sampling distribution is indicated by the triangles. Across-shelf stations are separated by 10 km and the 10 across-shelf transects (000 line through the 900 line moving southwest to northeast) are separated by 100 km. The 500 and 1000 m isobaths are indicated with the solid, and dotted lines, respectively. Geographic locations are abbreviated as: AdI-Adelaide Island, AnI-Anvers Island, DaB-Dallman Bay, EI-Elephant Island, GeS-Gerlache Strait, MaB-Marguerite Bay, ReI-Renaud Island and SSI South Shetland Islands.

designed to sample the region at least once a year with multiple cruises within certain years. The resulting hydrography is the most extensive, synoptic hydrographic data set for the west Antarctic Peninsula shelf waters to date and provides an excellent basis for the study of the region's physical properties. Investigations using these data are presented in Klinck and in Smith et al. [1999] and indicate that vertical heat fluxes may be dominated by the double diffusive instability and balanced by a slow and/or intermittent across shelf flux of heat from offshore. These concepts will be expanded and investigated further in this study.

The numerical modeling component of this research will consist of several process oriented studies and will involve the development of a vertical mixed layer model capable of including the effects of ice cover. This will be achieved by coupling a thermodynamic-dynamic ice model to the level 2.5 turbulence closure scheme [Mellor and Yamada, 1982] of the Princeton Ocean Model (POM), thus providing time dependent turbulent vertical mixing terms. This scheme has been found to reproduce realistic dynamics of the mixed layer [Blumberg and Mellor, 1987]. This model is used to evaluate the importance of vertical process on the structure of the mixed layer. These processes include the effects of wind driven turbulence mixing, surface buoyancy flux and double diffusion on vertical flux of heat and salt.

It is anticipated that this research will lend insight into the physical processes which influence the mixed layer dynamics of waters over the continental shelf west of the Antarctic Peninsula. Given the strong relationship between the physical environment in the region and biological processes, it is expected that this research will interest biologists. It is also believed that the oceanic response, and potential oceanic feedback into the coupled air/ice/sea system, will interest atmospheric scientists. The basic concepts explored in this research are fundamental to the development of models used to predict the response of the coupled physical-biological processes along the west Antarctic Peninsula to climatic change.

CHAPTER 2
BACKGROUND

The first section of this chapter gives a brief overview of the Palmer LTER program including its primary objectives, sampling grid, design and sampling strategy. The following section is a summary of previous hydrographic and circulation studies along the west Antarctic Peninsula. The third section provides a brief overview of meteorological and sea ice observations for the west Antarctic Peninsula region. The final section summarizes numerical modeling studies for the west Antarctic Peninsula region and adjacent seas and provides a general overview of ice-ocean modeling.

2.1 Palmer LTER program

The Palmer LTER program, based at Palmer Station on Anvers Island (Figure 1), has as a central hypothesis that interannual variability in the region's physical environment, in particular the extent of winter sea ice cover, drives interannual variability observed in the region's biology [Smith et al., 1995]. The program is multidisciplinary and includes components designed to collect, synthesize and model many of the physical and biological components of the regional environment and ecosystem, including the region's meteorology, sea ice, chemistry, hydrography and biology.

A sampling grid was established for the Palmer LTER [Waters and Smith, 1992] which extends 900 km along the west Antarctic Peninsula from the Bransfield Strait to Alexander Island (Figure 1). The offshore extent of the grid is 200 km. The grid is composed of 10 across-shelf transects with a 100 km separation. The southernmost across-shelf transect is designated the 000 line while the northernmost transect is the 900 line. A baseline connects the innermost stations on each across shelf transect and runs parallel to the peninsula. Following the Palmer LTER naming convention, a station which is 100 km away from innermost station on the 600 line would be referred to as the 600.100 station.

The offshore extent of the grid is sufficient to encompass the entire shelf which averages 400 m in depth. The 1000 m isobath (Figure 1) is the general location of the shelf break while the 500 m isobath demonstrates the highly irregular bathymetry of the shelf. The shelf is interrupted by several depressions which run from the outer to the inner shelf. One such cut intersects the 600 line to the west of Anvers Island (Figure 1) and provides a deep conduit for potential exchange of shelf waters with oceanic waters located offshore.

The basic sampling strategy for the Palmer LTER program includes an annual occupation the 200, 300, 400, 500 and 600 lines during the ice free summer months. During 1993, the region was sampled three times including cruises in the summer, fall and winter. The most extensive sampling was conducted as part of the fall cruise where the entire grid (000 to 900 lines) was sampled over a 2 month period. This fall cruise included a hydrographic survey with an across shelf resolution of 10 km and provided the most comprehensive, synoptic, hydrographic survey for the region to date.

2.2 Hydrography and circulation

The hydrography of the west Antarctic Peninsula was first mapped in the 1930's during the *Discovery* cruises to the Weddell-Scotia confluence and the Bransfield Strait [Clowes, 1934]. The northern shelf waters to the west of the Antarctic Peninsula (Figure 1) was revisited during 1970's as part of the International Southern Ocean Studies (ISOS) program [Gordon and Nowlin, 1978; Nowlin and Clifford, 1982; Sievers and Nowlin, 1984]. Interest in the region's biology initiated sampling through the 1980's as part of the First and Second International Biomass Experiments (FIBEX and SIBEX, respectively) [Stein, 1983; Stein and Rakusa-Suszczewski, 1983, 1984]. While the focus of the FIBEX and SIBEX programs was biological in nature, hydrographic data were collected. These data were generally restricted to the top 100 - 200 m of the water column, cluster around the Bransfield Strait, and do not extend south along the Peninsula.

Hydrographic results from the ISOS, FIBEX and SIBEX studies along the west Antarctic Peninsula can be summarized as follows: (1) The entire sub-pycnocline waters along the west Antarctic Peninsula shelf (excluding the Bransfield Strait) are characterized by warm, salty, oceanic water originating in the Antarctic Circumpolar Current (ACC) as Circumpolar Deep Water (CDW). (2) Within the Bransfield Strait, the deep waters lack the prominent, sub-surface temperature maximum characteristic of CDW and most likely originate along the western shelf of the Weddell Sea [Whitworth et al., 1994]. (3) The highly variable surface waters of the west Antarctic Peninsula are consistent with those of Antarctic Surface Water (AASW) which extend southward from the polar front to the Antarctic continent [Sievers and Nowlin, 1984].

In a review of historical data along the west Antarctic Peninsula, Hofmann et al. [1996] concluded that there is limited interaction between the deep waters of the Bransfield and those of the west Antarctic Peninsula. They also concluded that the west Antarctic Peninsula differs from other Antarctic shelf systems (e.g., Weddell and Ross Seas) as it does not appear to be a site of dense shelf water formation.

While little is known about the hydrography along the west Antarctic Peninsula, even less is known about its circulation. Drifter data indicate that the surface currents flow northward through the Gerlache and Bransfield straits, forming the Bransfield current [Niiler, 1990]. To date, few direct current measurements exist for the west Antarctic Peninsula shelf south of the Bransfield Strait. An estimate of the geostrophic currents, confirmed from limited hydrographic measurements, for the west Antarctic Peninsula are presented in [Stein, 1992] and suggest that weak cyclonic gyres may exist on the continental shelf.

2.2.1 Hydrographic observations from the Palmer LTER program

The most extensive, synoptic hydrographic data set along the west Antarctic Peninsula has been collected during several cruises that were part of the Palmer LTER program. These cruises were conducted in the austral summer, fall and winter of 1993, the austral summer of 1994 and the austral spring of 1991. Details on the data coverage and processing during the individual cruises are given in Klinck et al. [1994], Lascara et al. [1993a, 1993b] and Smith et al. [1993a, 1993b]. These hydrographic data have been used to develop a detailed descriptions of the water masses found along the west Antarctic Peninsula [Smith et al., 1999], thermohaline variability [Hofmann and Klinck, 1998] and changes in the heat and salt content of the water column during the 1993 sampling season [Klinck, 1998]. Results from these studies are summarized below.

The continental shelf waters along the west Antarctic Peninsula can be characterized as a two layer system which is separated by a distinct permanent pycnocline (Figure 2). The upper layer consists of the highly variable AASW which is in direct contact with the atmosphere and exhibits variability in its heat and salt content on seasonal (and shorter) time scales [Klinck, 1998; Smith et al., 1999]. The seasonal variability of AASW (Figure 3) is minimum in the winter and maximum in the fall. During this later period, the surface waters were characterized by multiple mixed layers at a wide range of temperatures and salinities [Smith et al., 1999]. Klinck [1998] calculates changes in heat content for the upper portion of the water column along the west Antarctic Peninsula using temperature data acquired during the 1993 and 1944 cruises to the west Antarctic Peninsula shelf. He demonstrates that AASW evolves from well mixed winter conditions (T $\sim$ -1.9 °C and S $\sim$ 34

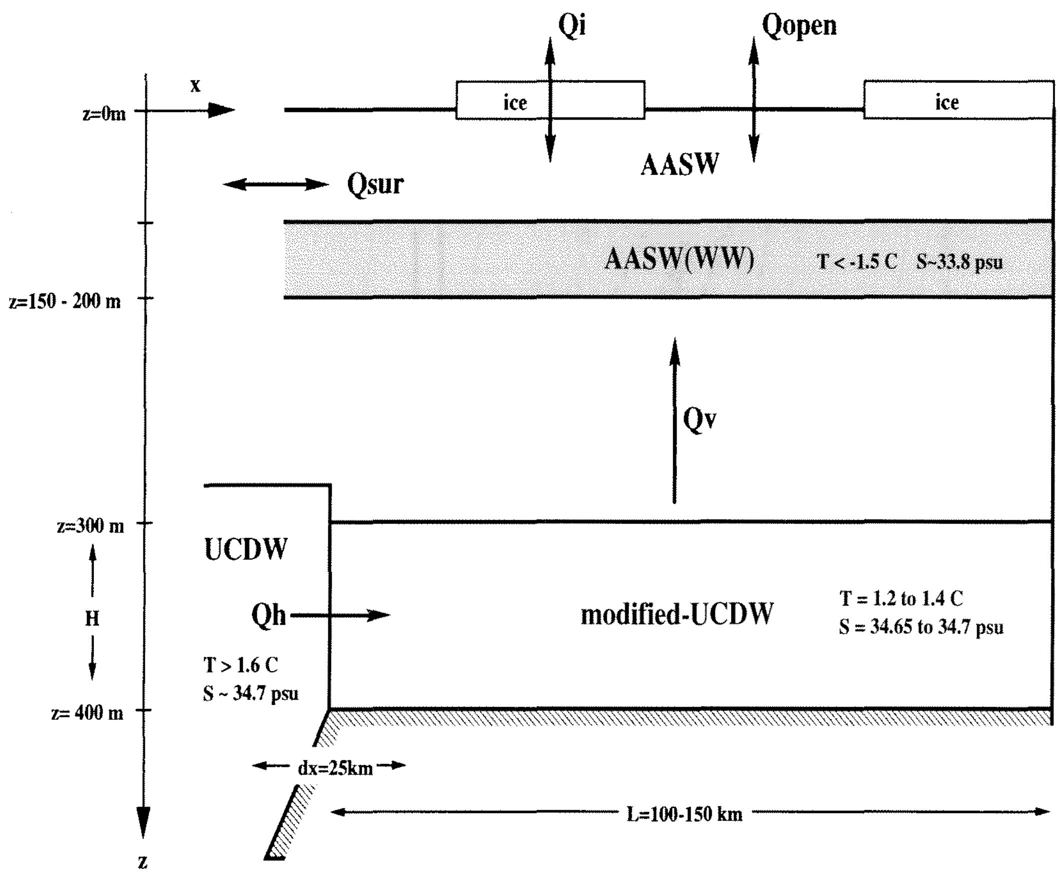

Figure 2. Schematic water mass distribution and box model. Antarctic surface water (AASW) and its end member, Winter Water (WW) occupy the top 100 to 200 m of the water column. The sub-pycnocline waters are UCDW and modified-UCDW which are located on the oceanic and shelf side of the shelf break, respectively. Arrows indicate potential mixing and water mass exchange pathways. Idealized shelf dimensions which are used in box model calculations for the shelf to quantify the individual heat fluxes (Q's), are indicated.

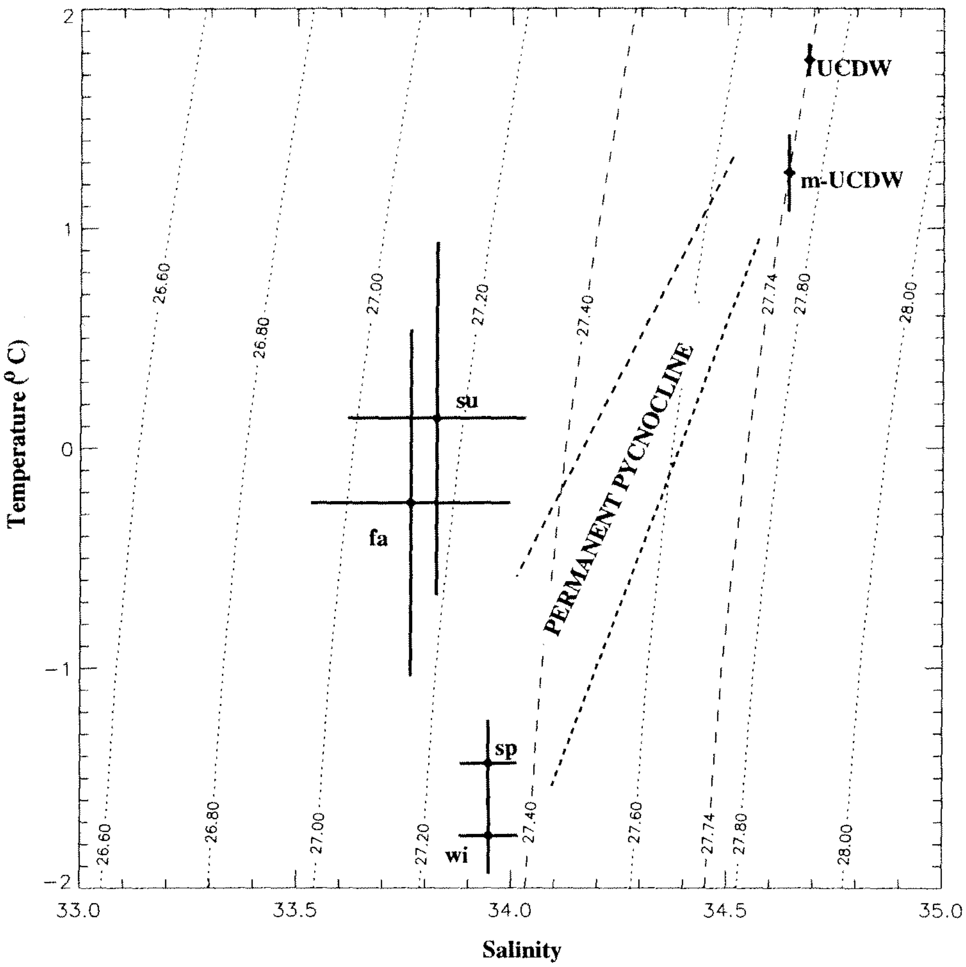

Figure 3. Hydrographic statistics from the Palmer LTER program. θ-S diagram from hydrographic data collected as part of the Palmer LTER program excluding the Bransfield Strait. The statistical envelopes found at $\sigma < 27.4$ represent surface θ-S means (± 1 s.d.) for a winter, spring, summer and fall cruise (wi, sp, su and fa, respectively). Combined θ-S means (± 1 s.d.) for the sub-pycnocline waters along $\sigma = 27.74$ are also indicated. The statistics for water with a temperature above 1.6 °C are labeled "UCDW" while the statistics for water below 1.6 °C are labeled as "m-UCDW" (modified-UCDW). Dashed lines show the general position of the permanent pycnocline. Constant density is indicated with curved dotted lines; the 27.4 and 27.74 isopycnals are indicated with dashed lines.

extending to a depth of 150 m) to summer, stratified conditions with an average heating rate on the order of 60 W m^{-2}.

Two key hydrographic features which characterize the surface layer are the depth of winter water (WW) and the depth of the mixed layer (*mld*). The coldest end member of AASW is termed WW and is the portion of AASW which is sufficiently deep to retain its temperature and salinity acquired during the previous winter [Mosby, 1934; Sievers and Nowlin, 1984] and forms a distinct temperature minimum just above the permanent pycnocline (Figure 4a). The *mld* is generally considered to be the maximum depth of surface mixing and is represented by the well mixed surface waters with uniform fairly uniform temperature and salinity (Figure 4a). The *mld* for the west Antarctic Peninsula shelf waters is controlled by stratification, wind mixing and buoyancy forcing associated with surface fluxes of heat and salt and is defined in this study to be the depth where the buoyancy frequency (N^2) exceeds an arbitrary threshold of 0.2×10^{-4} rad^2 s^{-2} (Figure 4b) (other thresholds can be used yielding similar results). During the winter, the mixed layer can extend to the top of the permanent pycnocline (i.e. to the depth of WW) (Figure 5e,f). During the spring, summer and fall, surface stratification resulting from surface heating and the input of fresh water results in shallow *mld's* (Figures 5a,c). Under conditions of surface stratification, a seasonal pycnocline can form between the mixed layer and WW (Figure 4a).

The sub-pycnocline waters along the shelf generally consist of warm, salty (T > 1.4 °C and S $\sim$ 34.7) water of oceanic, off-shelf origin (Figure 3). The statistics presented on the 27.74 isopycnal (Figure 3) indicate two things: 1) the sub-pycnocline waters form two distinct classes and 2) there exists little variability in their properties over time as indicated by the existence of two distinct clusters of data. The latter of these two observations is consistent with the temperature distributions from the historical record [Hofmann et al., 1996] which includes over 50 years of observa-

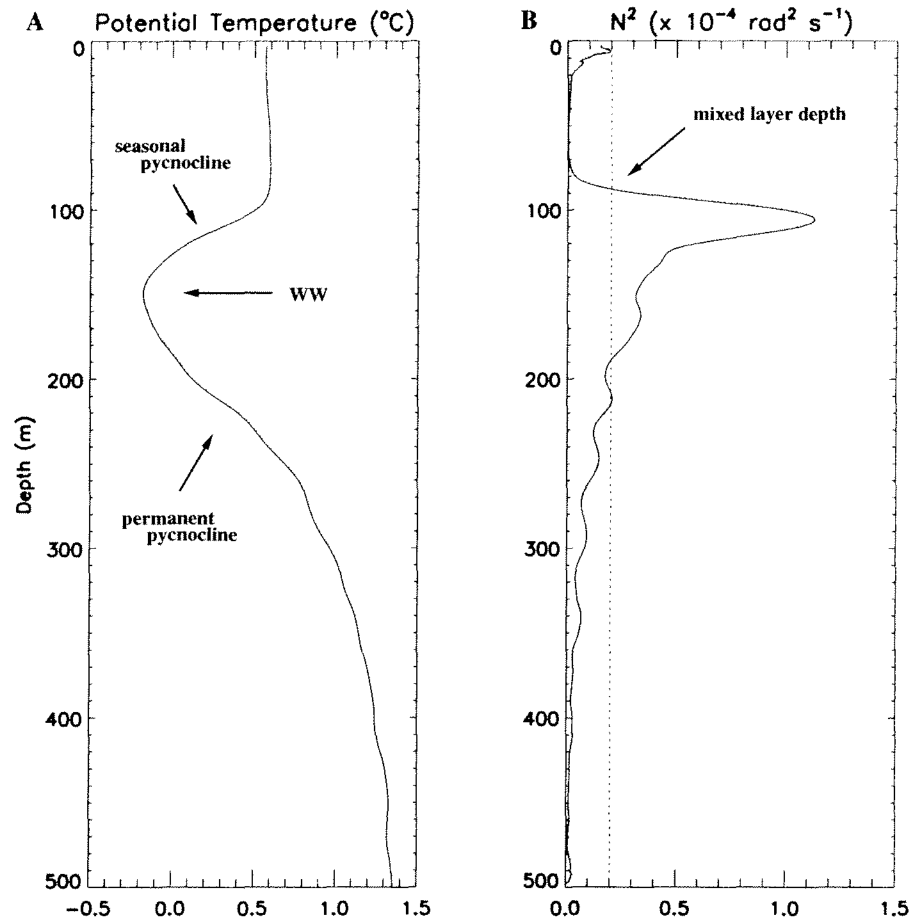

Figure 4. Fall 1993 potential temperature and buoyancy frequency versus depth for the 600.120 station. Vertical profiles of A) potential temperature (°C) and B) buoyancy frequency (N^2) (rad^2 s^{-2}) for the 600.120 station measured during Fall 1993. The temperature minimum indicates the depth of WW. The seasonal and permanent pycnoclines are labeled. The N^2 criteria used to determine mixed layer depths is indicated by the dotted line.

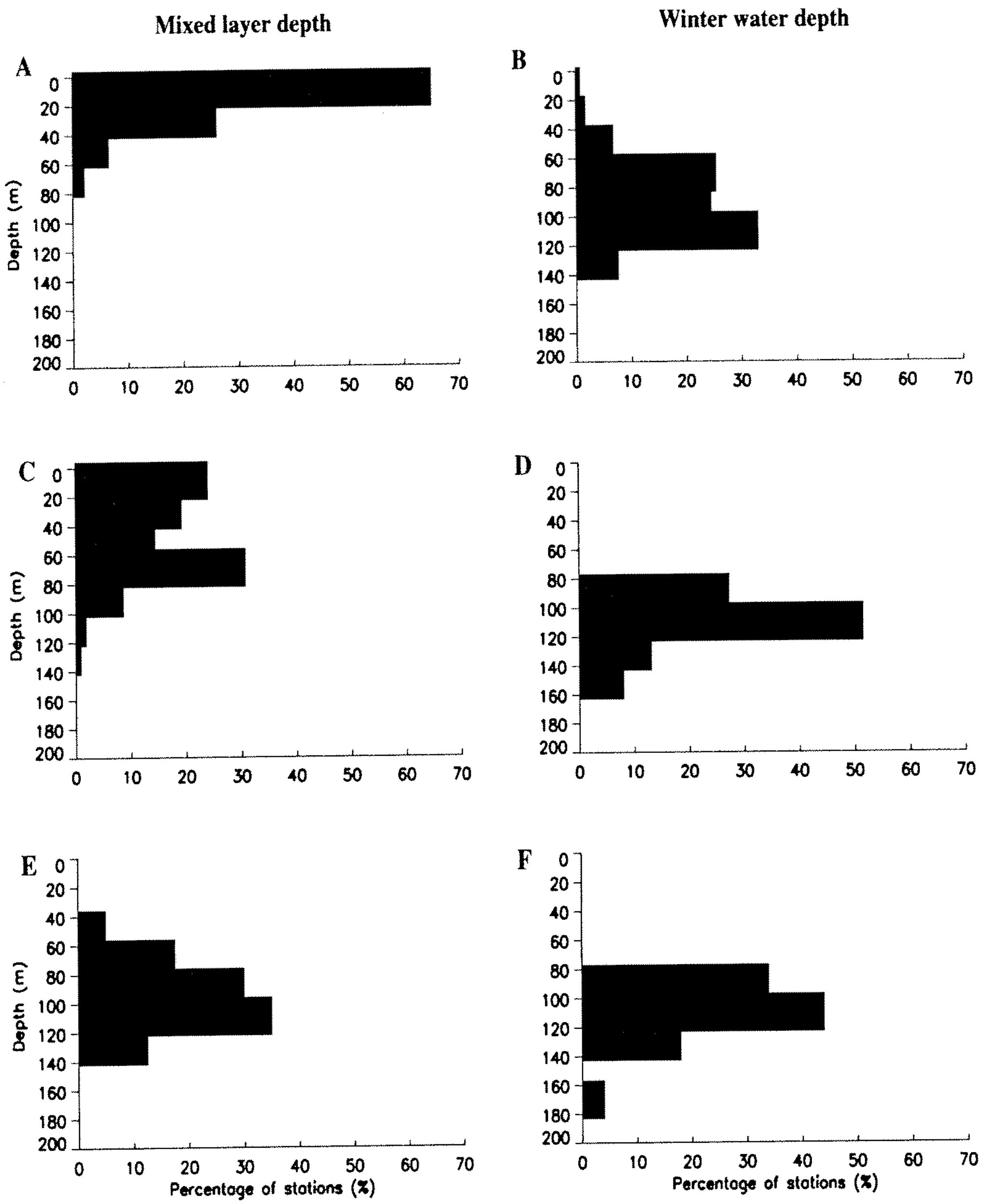

Figure 5. Frequency distributions for the winter water and mixed layer and mixed layer depths. A) Mixed layer and B) winter water depths were obtained from hydrographic observations made in January 1993. Mixed layer depths for C) March 1993 and E) August 1993 and Winter water depths for D) March 1993 and F) August 1993. The depth of the mixed layer is defined by the shallowest depth where the buoyancy frequency (N^2) exceeds 0.2×10^{-4} rad^2 s^{-2}. The analysis is based on all of the summer, fall and winter 1993 temperature and salinity data described in Section 3.1.

tions. The two classes are a warmer (T > 1.6°C) cluster from water on the oceanic side of the shelf break and cooler (1.2 < T < 1.4 °C) found on the shelf (Figure 2). This separation is statistically significant as the temperature mean of each group lies more than one standard deviation from the other mean. Smith et al. [1999] distinguish between these clusters calling the warmer group Upper-CDW (UCDW) and the cooler group modified UCDW. The modified version of UCDW is found over the shelf while unmodified UCDW was found only on the oceanic side of the shelf break and at stations influenced by the ACC. These observation indicate that the boundary of the ACC (thus the separation between UCDW and the modified UCDW) is generally within 20 km of the shelf break with a transition zone on the order of 10 to 25 km wide.

An analysis of historical hydrographic data which covers nearly 90 (1900-1990) years, presented in Hofmann et al. [1996] indicates that the separation between UCDW and the cooler version of UCDW found on the shelf persists over long time scales. Klinck [1998] and Smith et al. [1999] propose that the modified-UCDW is formed, and its hydrographic properties maintained, as UCDW from the ACC moves onto the shelf and looses heat (and salt) to overlying, cooler, fresher Winter Water (WW). Klinck [1998] and Smith et al. [1999] calculate the onshore flux of heat and salt necessary to balance vertical losses through the permanent pycnocline. The horizontal and vertical diffusive balances (Q_h and Q_v in Figure 2, respectively) that contribute to the formation of the modified version of UCDW can be expressed as

$$\begin{aligned} K_h^T \frac{H}{L}\frac{\partial T}{\partial x}|_{x=sb} - K_v^T \frac{\partial T}{\partial z}|_{z=py} &= \frac{1}{\rho_o C_p} I_H \\ K_h^S \frac{H}{L}\frac{\partial S}{\partial x}|_{x=sb} - K_v^S \frac{\partial S}{\partial z}|_{z=py} &= \frac{1}{\rho_o} I_S \end{aligned} \tag{1}$$

where I_H and I_S are the volume integrated heat and salt changes below the permanent pycnocline and the subscripts sb and py indicate that the terms are evaluated at the shelf break and across the pycnocline. The vertical and horizontal mixing coefficients for heat (T) and salt (S) are represented by K_v and K_h. In the Smith et al. [1999] study, the balance given by (1) is assumed to apply over the long term, background steady state and therefore assumes that I_H=I_S=0. Klinck [1998] used the above model to examine changes in the sub-pycnocline waters between seasons and evaluated I_H and I_S from observations. Using observed property distributions, Klinck [1998] and Smith et al. [1999] found that the hydrographic signature of modified UCDW on the shelf could be maintained with $K_H^T \sim K_H^S$ with values between 10 and 100 m^2s^{-1}. The most consistent balances were found when allowing for differences in the coefficients of vertical diffusion which would occur with double diffusion (i.e. $K_v^S = .1$ to $.3\ K_v^T$).

The two layer structure of the west Antarctic Peninsula continental shelf waters, and the formation of a distinctive permanent pycnocline (Figure 2) is different than many mid-latitude shelf systems where well mixed conditions extend throughout the water to the bottom. Klinck [1998] and Smith et al. [1999] speculate that one possible explanation for the oceanic character of the sub-pycnocline shelf waters along the west Antarctic Peninsula is the rather deep shelf which is generally greater than 400 m thus allowing oceanic water to intrude (Figure 1). The lack of cold, dense shelf water may also result from the relatively warm atmospheric conditions and/or the absence of large permanent ice shelves in the region.

2.3 Meteorology and sea ice

Meteorological conditions are important in determining water mass distribution and the dynamics of the mixed layer. Obvious meteorological contributions to mixed layer dynamics are wind driven Ekman circulation and buoyancy forcing from atmospheric fluxes of heat and fresh water. Also, in high latitude systems the atmospheric heat flux plays a crucial role in sea ice formation.

The surface waters of the west Antarctic Peninsula continental shelf region vary from nearly ice-free ($< 10\%$ coverage) in the austral summer to fully ice covered (nearly 100% coverage) in the austral winter [Stammerjohn and Smith, 1996]. Furthermore, the extent of maximum winter ice cover, and the timing of the advance and retreat of ice, is variable from season to season [Stammerjohn and Smith, 1996], and interannual variability in the extent of winter ice coincide with variations in the mean winter temperatures. These warm and cold atmospheric conditions result in low and high ice years, defined relative to the average ice conditions over time.

Smith et al. [1996] use atmospheric data from Faraday Station to demonstrate that climatic conditions along the western side of the Antarctic Peninsula are characterized as a maritime climate which is generally warmer than the Weddell side. They also indicate that the temperatures exhibit a meridional gradient (especially in the winter) where temperatures along the southern portion of the Antarctic Peninsula are cooler than in the north near the Bransfield Strait. This temperature gradient breaks down in the summer giving way to a more uniform distribution. Smith et al. [1996] also use data from a mid-shelf automatic weather station (AWS) (i.e. located about 100 km from the Antarctic Peninsula near the 600 line) to show that atmospheric conditions differ from onshore to offshore. The differences between onshore and offshore atmospheric conditions is also demonstrated by Klinck and Smith [1995] where station meteorology is compared to ship-based observations during the 1993 LTER fall cruise. Land-based meteorological data (i.e. from Palmer and Faraday) is influenced by local topography (especially the wind data) which may account for a large part of the across-shelf differences. While the mid-shelf data may represent conditions on the shelf more realistically than the station data, the record is rather short (1 year). The mid-shelf data set also contains many data gaps. Because of these problems, data at the peninsula stations will be used in this study.

2.4 Circulation modeling studies for the west Antarctic Peninsula region

2.4.1 Regional modeling studies

Capella [1989] adapted the three-dimensional, primitive equation model of Semtner [1974] to simulate ice-free circulation around the Bransfield Strait and South Shetland Islands. His results indicate a northeastward wind-driven surface flow which is sensitive to seasonal changes in the wind field. He also demonstrates a region of complex circulation near Elephant Island, which most likely results from an interaction of the wind driven flow and the complex bathymetry. Capella [1989] did not include sea ice effects on the circulation and the southern boundary of his model (periodic with the northern boundary) only extended to the northern portion of the west Antarctic Peninsula shelf. Even with these limitations, the general magnitude and direction of the simulated flow fields presented by Capella [1989] provide some context for evaluating the results of this study.

The Fine Resolution Antarctic Model (FRAM) [FRAM Group, 1991; Webb et al., 1991] provides simulated circulation fields for the entire Southern Ocean on a 2.5 by 2.5 km grid and reproduces many of the key circulation features such as the general location and transport of the ACC. However, the simulated circulation for the west Antarctic Peninsula shelf region is questionable [Hofmann et al., 1996]. The realism of the model solutions in this region is affected by the smoothed bathymetry used in the model. The west Antarctic Peninsula shelf bathymetry is poorly represented. Also, the FRAM circulation does not directly include sea ice processes.

2.4.2 Coupled sea ice-ocean models

Sea ice models are generally divided into thermodynamic sea ice models and coupled dynamic-thermodynamic sea ice models. The former predicts sea ice growth and melting as a function of the imbalance between imposed atmospheric heat fluxes and the calculated heat flux through the ice [Maykut and Untersteiner, 1969; Semtner 1976]. The latter couples ice growth from a thermodynamic model to wind and current-driven ice motion. The most complex sea ice models include the effects of internal ice stress on ice motion and thickness by including a numerical treatment of ice rheology (e.g., Hibler [1979]). However, Hibler [1979] and Ikeda [1989] indicate that rheology is unnecessary for thin, new ice with areal coverage less than 80%, conditions which generally apply to the shelf waters along the West Antarctic Peninsula [Stammerjohn and Smith, 1996].

Coupled sea ice-ocean models of the Weddell Sea [Hibler, 1979; Lemke, 1987; Lemke et al., 1990; Stossel et al., 1990], the Bering Shelf system [Kantha and Mellor, 1989; Mellor and Kantha, 1989] and the Arctic [Häkkinen and Mellor, 1990] have been used to demonstrate the importance of sea ice processes and thermodynamics on circulation and mixed layer at high latitudes. While none of these models specifically address the shelf waters of the west Antarctic Peninsula, the results from these studies are used to formulate models for the region. Specifically, Kantha and Mellor [1989] couple a thermodynamic sea ice model, based on the Semtner [1976] model, to the Mellor and Yamada [1982] level 2.5 (MY2.5) turbulence closure scheme used in the Princeton Ocean Model (POM). The model was later enhanced by Häkkinen and Mellor [1990] and is hereafter referred to as the MKH model. The coupling in the MKH model involves the parameterization of physics in the molecular sub-layer at the ice-water interface, which transfers heat and salt between the ice and ocean models. This parameterization was found to have a significant effect on sea ice thermodynamics. Much of their work provides the basis for the sea ice - mixed layer development in this study.

CHAPTER 3

DATA AND METHODS

This chapter provides details of the datasets, analysis methods and numerical model used to estimate heat budgets and assess the physical processes contributing to the mixed layer structure of the west Antarctic Peninsula shelf waters.

3.1 Data sets

The temperature and salinity data collected from four cruises that occurred on the west Antarctic Peninsula continental shelf along with meteorological data from two land-based stations (Faraday and Palmer) are used to construct regional heat budgets and to initialize and validate a sea ice-mixed layer model. The meteorological data from Faraday Station consists of daily observations of air temperature, relative humidity, atmospheric pressure and wind speed and direction. Sea surface temperatures and solid precipitation records (described in Section 3.4.5) from Palmer Station were also used in the heat budget and sea ice mixed layer model. Meteorological variables from a National Center for Environmental Prediction (NCEP) and National Center for Atmospheric Research (NCAR) 40 year data re-analysis [Kalnay et al., 1996] were used to obtain larger spatial cover. Daily records are limited to the year 1993, but monthly values are reported for the entire 40 year time span. Sea ice concentrations used in this study were derived from the recently re-distributed global sea ice concentration grids from the National Center for Snow and Ice Data Center (NCSID).

3.1.1 Hydrographic data

Between January 1993 and February 1994, portions of the west Antarctic Peninsula shelf were sampled during four cruises (details in Table 1). The fall (March-May) 1993 cruise included the entire area between the 000 and 900 (Figure 1) and provided

Table 1. Season, dates, and region covered for the west Antarctic Peninsula cruises used in this study.

LTER Cruise ID	Season	Dates (dd-month yy)	Lines Sampled
93A	summer	08-Jan 93 to 07-Feb 93	200-600
93B	fall	25-Mar 93 to 15-May 93	000-900
93C	winter	23-Aug 93 to 30-Sep 93	200-600
94A	summer	11-Jan 94 to 07-Feb 94	300-600

the most extensive, synoptic hydrographic observation for the region to date. The 200 through 600 lines were occupied during the summer 1993 (January-February) and the winter 1993 (August-September). During the summer of 1994, the 300 through 600 lines were occupied providing hydrographic data for two consecutive summer seasons.

On all cruises, conductivity-temperature-depth (CTD) measurements were made with a 20 km across-shelf resolution using a SeaBird CTD mounted on a Bio-Optical Profiling System (BOPS) [Smith, 1984] to within 20 m of the bottom, or to 500 m in deeper water. On the fall 1993 cruise, a SeaBird 911$^+$ was also deployed to obtain 10 km resolution in hydrographic properties. During the fall cruise, CTD casts were made to depths of 20 m above the bottom, or to 4000 m for deeper water. Water samples were taken at discrete depths and analyzed for salinity with a Guideline Salinomenter calibrated with IAPSO standard sea water. During the fall cruise, frequent cross-sensor comparisons were made. Additionally, pre- and post-cruise calibrations were made by SeaBird Electronics. No significant sensor drift was determined in time or with depth; thus, no corrections were made to the original data. Derived data products were calculated using algorithms given in UNESCO [1993]. Full details on data collection and processing for each cruise are given in Klinck et al. [1994], Lascara et al. [1993a, 1993b] and Smith et al. [1993a, 1993b].

3.1.2 Meteorological and radiation data from Faraday Station

Atmospheric observations from Faraday Station, made by British Antarctic Survey (BAS) personnel, are archived at the University of Wisconsin. The Faraday data are the longest, most consistent and highest quality measurements of atmospheric conditions for the region to the west of the Antarctic Peninsula. The data span the years from 1957 to 1993 and include observations of dry and wet bulb air temperatures (°C), cloud cover (%), wind speed (m s^{-1}), wind direction (° from N), relative humidity (%) and atmospheric pressure at the sea level (mb) taken at 3 hour intervals. Details on BAS data sets, collection techniques, data processing and sensor calibrations can be found in Jones and Limbert [1987]. The Faraday observations were used to calculate daily averages for all meteorological parameters which were used to estimate surface fluxes of heat and salt. These fluxes are also used as input to the sea ice-mixed layer model. Observations of surface radiation, including hourly records of total short wave radiation (W m^{-2}), are available from BAS for the years of 1985 through 1993.

Estimation of the flux of short wave radiation at the ocean's surface are needed in the calculation of the surface, ice free heat budget (Section 3.2) and for input into the sea ice-mixed layer model (Section 3.3). The contribution of short wave radiation to the heat budget is estimated by applying a cloudiness factor derived by Laevastu [1960] to the clear-sky, geometric model of Zillerman [1972].

The equation for clear-sky, short wave radiation (Q_{sw}^{clear}) (W m^{-2}) is

$$Q_{sw}^{clear} = \frac{S_c\ cos^2 Z}{10^{-5}(cosZ + 2.7)e_A + 1.085\ cosZ + 0.1} \tag{2}$$

where S_c (Table 2) is the solar constant and e_A is the atmospheric vapor pressure (calculated from relative humidity). The cosine of the solar zenith angle (Z) is given by

$$\cos Z = \sin\phi\ \sin\gamma\ +\ \cos\phi\ \cos\gamma\ \cos\Psi \tag{3}$$

where ϕ is latitude (ϕ=65°S in this study). Solar declination (γ) and the hour angle (Ψ) are given, respectively, by

$$\gamma = 23.44^\circ \ \cos\left[360^\circ(172 - \mathit{year\ day})/365\right] \tag{4}$$

and

$$\Psi = 15^\circ \ (12 - \mathit{solar\ time}) \tag{5}$$

Total short wave flux at the surface (Q_{sw}) is then estimated by reducing Q_{sw}^{clear} (2) by a cloudiness factor [Laevastu, 1960].

$$Q_{sw} = Q_{sw}^{clear}\left(1 - 0.6\ C_t^3\right) \tag{6}$$

where C_t is cloud cover in tenths of sky obscured.

The short wave radiation record at Faraday is a direct measurement at the earth's surface and contains information about the clouds thus providing an excellent record to verify and calibrate the cloudiness correction and the clear-sky model. Comparisons between calculated short wave radiation and the direct measurements from Faraday (Figure 6) indicate that (2) and (6) accurately reproduce the time variability of the short wave radiation at this location. The model-data comparison (Figure 6) indicates that, no tuning of these equations is necessary and therefore the simulated short wave radiation time series was used as input to the sea ice-mixed layer model.

3.1.3 Sea surface temperature near Palmer Station

A daily record of sea surface temperatures (SST) for the waters surrounding Palmer Station for the years 1992-1994 was calculated by combining surface data from ship observations near Palmer Station (50 km radius) with records obtained from an AWS located at Bonaparte Point (65°15'S, 64°15'W). This combined data set was averaged to give daily values. Quadratic curves were fit to the spring, summer and

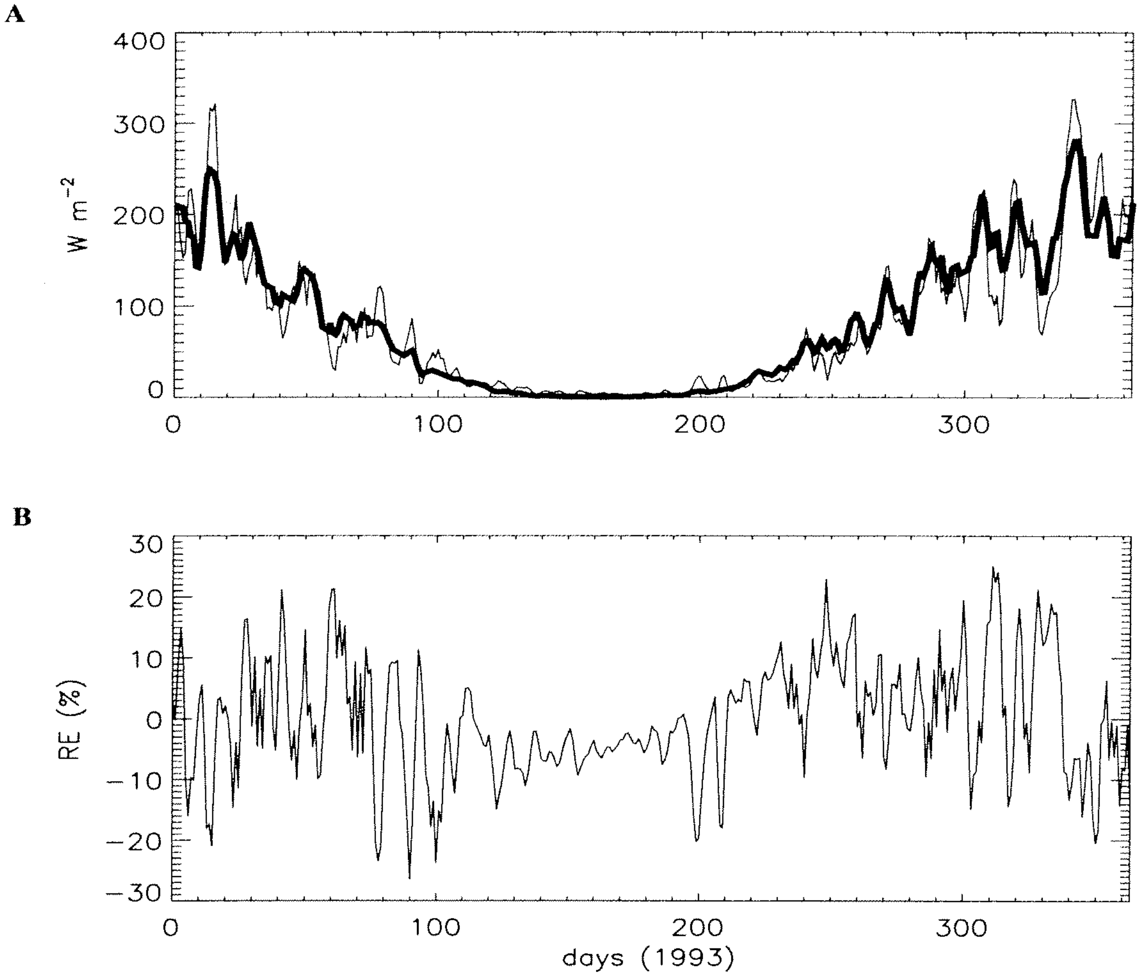

Figure 6. Comparison of calculated and measured surface, short wave radiation flux. A) Comparison between the short wave radiation flux (W m^{-2}) calculated from the Zillerman [1972] and Laevastu [1960] equations (thick line) and a direct measurements made at Faraday Station (thin line). Measured and calculated averages for the year are 84 and 82 W m^{-2}, respectively. B) Relative error (RE) for measured and calculated short wave radiation fluxes (Q_{sw}^{meas}, Q_{sw}^{calc}). RE= 100.*(Q_{sw}^{calc}-Q_{sw}^{meas})/ (Q_{sm7}^{meas}), where Q_{sm7}^{meas} is the measured short wave radiation data smoothed with a 7 point smoother. The average RE=-1.3 %.

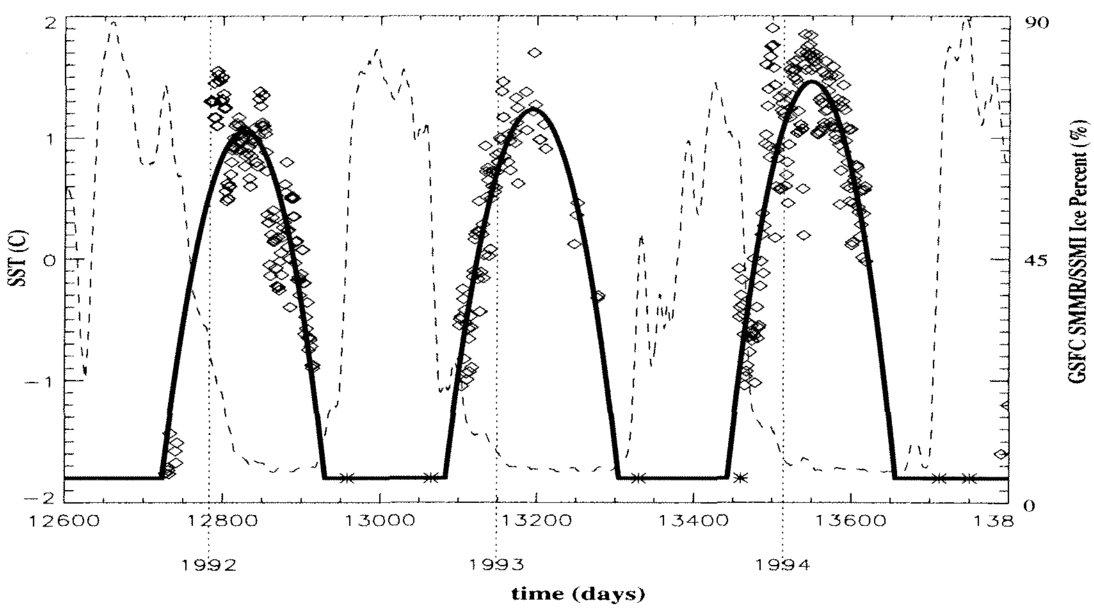

Figure 7. SST record for the Palmer Basin (50 km radius around Palmer Station) for 1992-1994. Diamonds indicate daily average surface temperatures computed from Bonaparte Point AWS and surface temperature and salinity from ship observations. The thick solid line represents a curve fit to the data. The dashed line is the GSFC SMMR/SSMI derived sea ice concentration which are used to set the SST to the freezing point of sea-water with salinities typical of those along the west Antarctic Peninsula shelf (SST=-1.9°C). The x-axis represents the Julian day since January 1, 1957 (January 1 of each year are indicated with vertical dotted lines).

fall observations to produce a continuous daily record. Winter SST conditions were assumed to be freezing (T_f=-1.9°C) during times when satellite-derived (Section 3.1.5) sea ice distributions indicated that the region around Palmer Station had at least 20% ice cover. The daily averaged SST observations and the resulting continuous SST record, along with the satellite derived ice fields used to determine winter SST's, are presented in Figure 7. The diamonds in the figure represent the daily observations while the solid black line represents the derived SST record. Periods of constant SST at the freezing point coincide with periods of ice cover (as indicated by the dashed line). Summer SST's range between 1 and 2 °C. These summer temperatures are consistent with the observations the inner-station data presented in Smith et al. [1999]. The smooth SST curves produced by this method averages over high frequency variability observed in the daily observations; however, this method is conservative and does not produce false peaks associated with more elaborate methods of producing continuous daily records (e.g. spline fitting techniques). The fitted SST data appear to underestimate the summer peak temperatures; however, it will be shown in Section 4.1.2 that the total heat budget is not very sensitive to the choice of SST.

3.1.4 Meteorological data from the NCEP/NCAR reanalysis project

A globally gridded (2.5×2.5°) atmospheric data set from a joint project between the National Center for Environmental Prediction (NCEP) and the National Center for Atmospheric Research (NCAR) provides various atmospheric parameters on 17 different pressure levels (including sea-level) for a 40 year (1957-1996) time span [Kalnay et al., 1996]. Their global reanalysis model assimilates global distributions of land-based and ship based meteorological observations. An advantage of this technique, described in Kalnay et al. [1996], is that the numerical procedure remained essentially unchanged during the entire analysis eliminating apparent climate shifts which arise from using various techniques during a simulation.

Daily atmospheric data for the 1993 and monthly averages for the entire simulation were obtained from NCEP and NCAR for use in this study. Daily values are available for the entire 17 year simulation but such detailed analysis was beyond the scope of this study. Atmospheric pressure (mb) and air temperature (°C) at sea level were extracted for a geographic region around Drake Passage (10° to 180°W and 30° to 85°S) and were used to identify larger-scale spatial patterns which may affect interpretations of ocean heat and sea ice budgets (Section 5.2).

3.1.5 Sea ice from the SMMR and SSMI

A 17-year record of sea ice concentrations for the west Antarctic Peninsula shelf was extracted from the National Snow and Ice Data Center (NSIDC) archives [Cavalieri et al., 1997]. The NSIDC data is a combination of three previous data sets which have been cross-calibrated at NASA Goddard Space Flight Center (GSFC) [Comiso et al., 1997]. This record is the longest, most continuous global record of sea ice distributions to date. The individual sea ice records are from the Nimbus 7 Scanning Multichannel Microwave Radiometer (SMMR) satellite which operated from October 1978 to August 1987. The second and third records are derived from the Defense Meteorological Satellite Program's Special Sensor Microwave/Imager satellite (F8 and F11 SSM/I), providing data coverage from July 1987 to December 1991 and from December 1991 to September 1995, respectively. Comiso et al. [1979] use time overlaps to cross-calibrate the individual time series. These calibrated data are referred to as either the GSFC SMMR/SSMI sea ice record or the observed ice fields when used in this study.

The equal area (625 km^2) GSFC SMMR/SSMI sea ice grid in the vicinity of the west Antarctic Peninsula is illustrated in (Figure 8). This grid consists of sea ice data with east-west and north-south positions given by i and j locations, respectively.

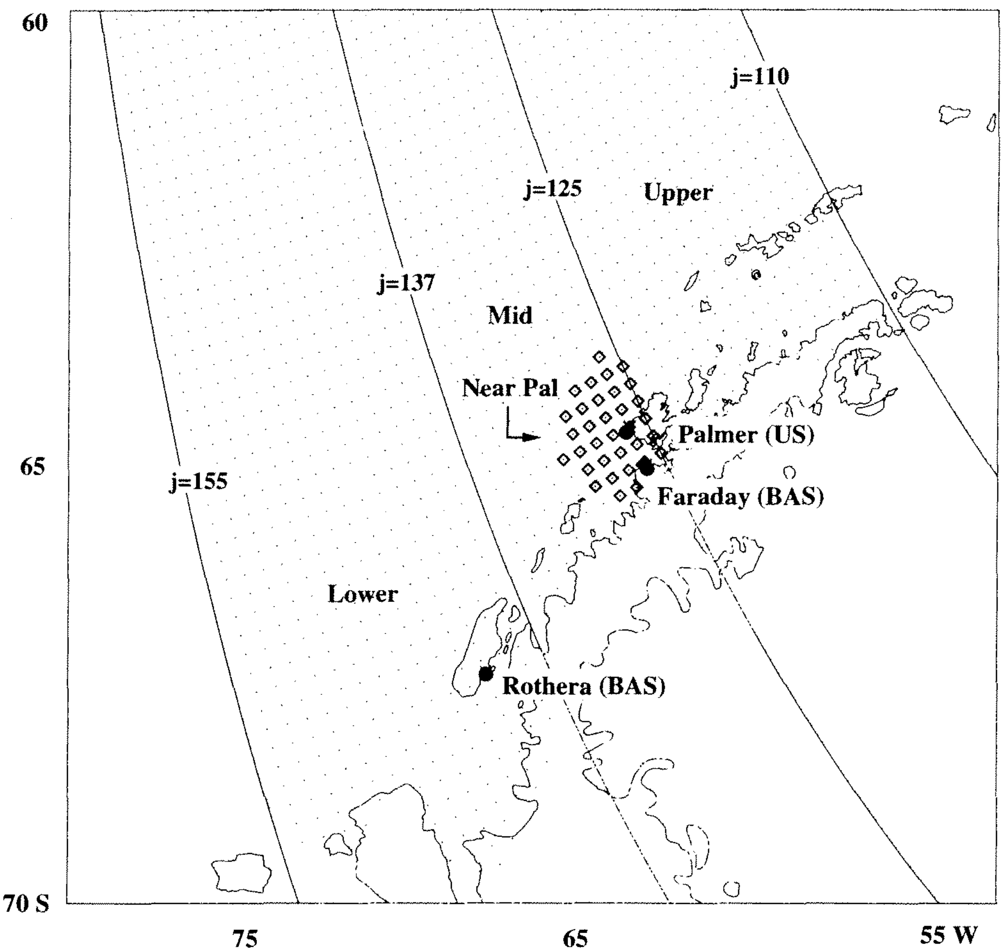

Figure 8. The west Antarctic Peninsula and the GSFC SMMR/SSMI sea ice concentration grid (indicated with dots). The GSFC SMMR/SSMI grid is an equal area grid (625 km^2) with east-west and north-south gird locations given by i and j indexes, respectively. The j index is used to define the northern (j=110) and southern (j=155) boundaries of the grid for use along the west Antarctic Peninsula. Similarly, lines of constant j index are used to partition the region into a lower-, mid- and upper-region. GSFC SMMR/SSMI data locations within 50 km of Palmer Station are indicated with diamonds.

The GSFC grid is area preserving and the i,j pairs do not correspond to consistent longitude and latitude locations, thus resulting in the distortion noticed in Figure (8) when projecting the GSFC SMMR/SSMI grid onto the cylindrical map used to represent the west Antarctic Peninsula shelf.

The northern and southern extent for data extracted for use in constructing a west Antarctic Peninsula shelf time series are given by GSFC SMMR/SSMI j indexes of j = 155 (south) and j=110 (north), respectively (Figure 8). The eastern extent of the region is defined by the Antarctic Peninsula. No offshore (westward) grid extent was specified, which allows all sea ice between the peninsula and the ice edge to be included in the analysis.

Sea ice area for a given cell ($A_i^{(i,j)}$) is calculated by multiplying the percentage ice cover for the cell by its total area (i.e. 625 km^2 for all cells). For a given day, the total ice area for the west Antarctic Peninsula region by summing all $A_i^{(i,j)}$ over the grid presented in Figure (8) bounded by the j indices described above. The time series for ice area (Figure 9b) is then produced by repeating the above summation for all daily records in the GSFC SMMR/SSMI record.

In addition to the total sea ice area for the west Antarctic Peninsula, 4 sub-sets of sea ice time series were extracted to give information for different regions along the shelf as well as near Palmer (Figure 8). The north-south GSFC SMMR/SSMI grid index (i.e. j index) is used to define these sub-sets as follows: lower [$138 < j < 155$], middle [$126 < j < 137$] and upper [$138 < j < 155$] regions (Figure 8). In addition to total ice record and the lower-, mid- and upper- regions, a near-Palmer record consisting of data within 50 km of Palmer Station (indicated with diamonds in Figure 8) was also extracted. The near Palmer record is used frequently to compare model derived sea ice to observations.

Smith et al. [1996] compares a similar sea ice record to air temperatures recorded at Faraday Station and concludes that there is a relationship between cold/warm wintertime atmospheric temperatures and high/low ice years. This result is quantitatively similar to trends observed in (Figure 9) with high ice years in 1980 and 1987 corresponding to cold air temperatures. The lowest ice year on record (1989) corresponds to the winter with the warmest atmospheric conditions. These relationships will be investigated further in this study.

3.2 AASW heat flux calculation

The total heat and salt budget for AASW (schematically represented in Figure 2) include surface fluxes through the atmosphere-AASW interface, ice-AASW interface and vertical fluxes through the permanent pycnocline.

The surface heat budget for the AASW layer west Antarctic Peninsula is calculated by assuming that through ice heat fluxes are negligible when compared to the heat fluxes in the open-water, ice-free regions (i.e. $Q_{open} > Q_{ice}$ in Figure 2). Under this assumption, the total heat flux is represented by the ice-free budget which is calculated by combining bulk aerodynamic estimates of latent and sensible heat fluxes (Section 3.2.1) with contributions from short- and long-wave radiation. The short- and long-wave radiation budgets are calculated from geometric equations commonly used in numerical modeling studies (e.g. Parkinson and Washington [1979]) (Section 3.1.2 and 3.2.1).

Vertical heat and salt fluxes from warm, salty sub-pycnocline waters found at depth along the shelf are estimated using the double diffusive model presented by Marmorino and Caldwell [1976] (MC76 model) (Section 3.2.2). Klinck [1998] and Smith et al. [1999] indicate the transfer of heat and salt through the permanent pycnocline is enhanced, and possibly governed, by process of double diffusion.

The AASW heat budget described above only accounts for vertical processes at the atmosphere-AASW interface and vertical fluxes of heat through the permanent pycnocline. Horizontal contributions of heat and salt (i.e. Q_{sur} in Figure 2) are

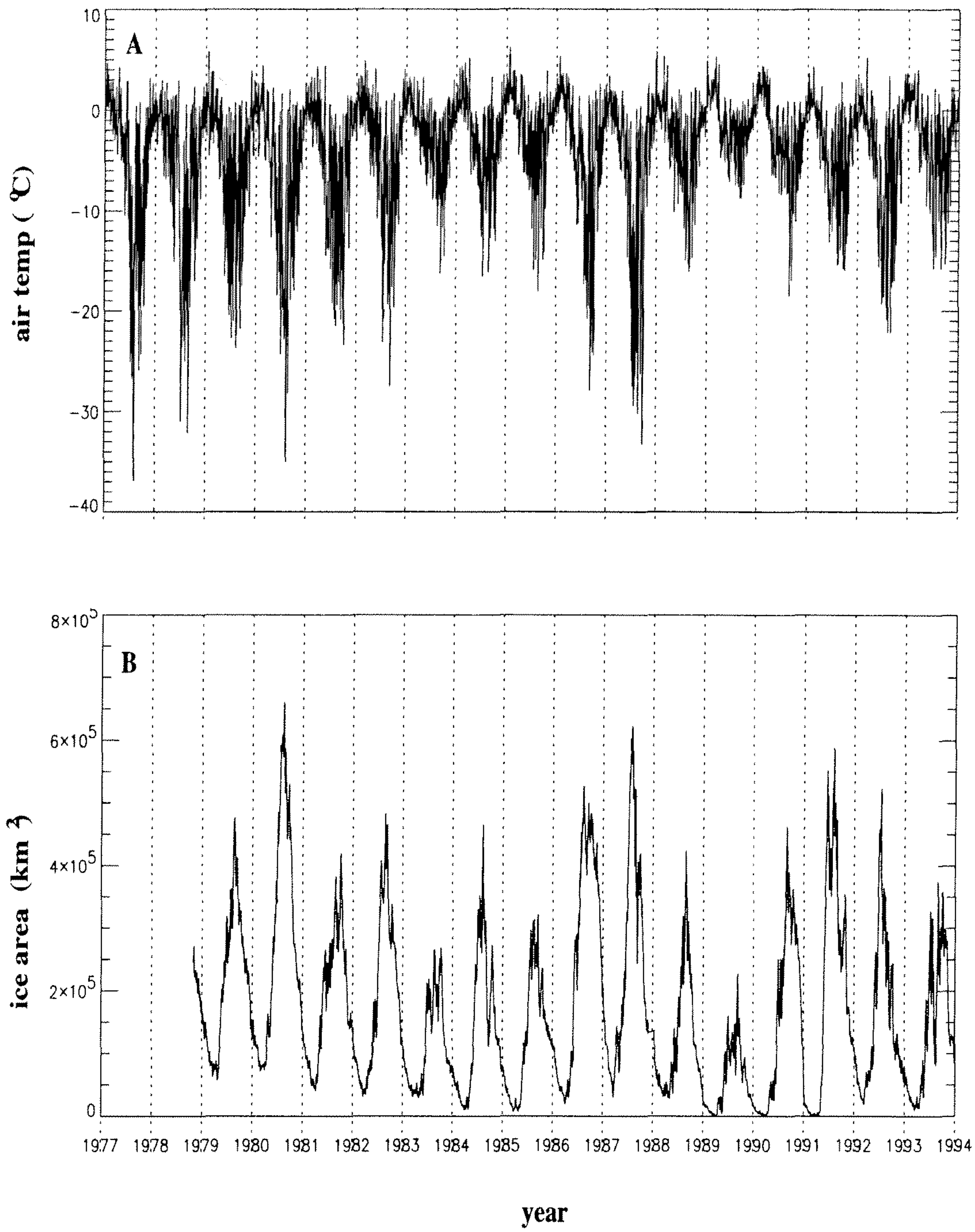

Figure 9. A) Air temperatures observed at Faraday Station and B) Extracted GSFC SMMR/SSMI sea ice time series. Vertical dotted lines indicate January 1 of each year.

not included in the calculation. These processes will be addressed in the modeling portion of the study along with the contribution of heat fluxes at the sea ice-AASW interface (Section 3.4.5) which are also neglected in this ice-free calculation.

3.2.1 Surface, ice-free heat flux calculation

The total heat exchange (Q_{tot}) (W m^{-2}) across the air-sea ice interface is estimated as

$$Q_{tot} = (1 - A_i)Q_{open} + A_i \cdot Q_{ice} \tag{7}$$

where Q_{open} is the ice-free, open ocean heat exchange, Q_{ice} represents heat exchanges through the sea ice and A_i is the ice concentration obtained from the daily, near-Palmer GSFC SMMR/SSMI ice record (Section 3.1.5). The determination of Q_{open} is fairly straightforward and involves using observations of meteorological and oceanic data. Estimating Q_{ice} requires measurements of ice thickness (h_i), the skin temperature of ice and surface albedo and which are not commonly available.

In high latitude systems, open ocean heat fluxes are often orders of magnitude greater than through-ice heat fluxes even in regions characterized by 98% ice cover [Parkinson and Washington, 1979]. Thus, an initial estimate for the regional heat budget for the shelf waters will assume that the ice acts as a perfect insulator blocking all heat transfer between the ocean and atmosphere (i.e. $Q_{ice} = 0$). This assumption will be relaxed, and evaluated, in the modeling section of the study where through ice heat fluxes are calculated.

Assuming that heat exchanges through the ice are zero, the ice-free flux at the air-sea interface (Q_{tot}) can then be estimated as

$$Q_{tot} = (1 - A_i) \cdot [(1 - \alpha_s) \cdot Q_{sw} + \epsilon \cdot (Q_{lw}^{back} - Q_{lw}^{down}) + Q_{sens} + Q_{lat}] \tag{8}$$

where Q_{sw} represents the heat input into the surface water from total incoming short wave radiation, given by equations (2) and (6), and α_s is the surface albedo (Table 2).

The upward longwave radiation (Q_{lw}^{back}) is calculated from the Stefan-Boltzmann relationship

$$Q_{lw}^{back} = \sigma \left(SST + 273\right)^4 \tag{9}$$

where ϵ is the surface emissivity and σ is the Stephan-Boltzmann constant (Table 2). Daily sea surface temperatures from near Palmer Station were used to specify SST (Section 3.1.3).

Incoming longwave radiation (Q_{lw}^{down}) is estimated from air temperature, T_{air} (°C) and cloud cover, C_l.

$$Q_{lw}^{down} = \sigma \left(T_{air} + 273\right)^4 \cdot \left(0.7855 + 0.2232 \cdot C_l^{2.75}\right) \tag{10}$$

Sensible heat exchange (Q_{sens})is estimated with a bulk aerodynamic formula for heat transfer

$$Q_{sens} = \rho_a C_{pa} C_{HO} W \left(T_{sst} - T_{air}\right) \tag{11}$$

where c_{pa} and ρ_a are the specific heat of air at constant pressure and the density of air, respectively and W is the wind speed (m s^{-1}) The heat transfer coefficient (C_{HO}) (Table 2) is chosen to be consistent with the MKH model.

Latent heat exchange (Q_{lat}) is calculated from

$$Q_{lat} = \rho_a L_v C_{HO} W \left(q_o - q_A\right) \tag{12}$$

where L_v is the latent heat of vaporization, q_A and q_o are the specific and the saturated specific humidities, respectively.

3.2.2 Double diffusive heat and salt flux

A second source of heat and salt to AASW is the relatively warm, salty, sub-pycnocline waters found below 100 m on the shelf to the west of the Antarctic Peninsula [Hofmann and Klinck, 1998] (c.f. Figure 2). These waters are a modified version of oceanic UCDW and are consistently found along the shelf. The

Table 2. Constants used in the heat flux calculations and numerical model.

Symbol	Variable Name	Value
ρ_a	density of air	1.3 kg m^{-3}
ρ_i	density of ice	900 kg m^{-3}
ρ_o	density of water	1028 kg m^{-3}
g	gravitational acceleration	9.8 m s^{-2}
k_i	thermal conductivity (ice)	2.04 J m^{-1} s^{-1} K^{-1}
k_s	thermal conductivity (snow)	0.33 J m^{-1} s^{-1} K^{-1}
L_v	latent heat of vaporization	2.501×10^6 J kg^{-1}
L_f	latent heat of fusion	3.347×10^5 J kg^{-1}
k_t	molecular diffusivity (heat)	1.4×10^{-7} m^2 s^{-1}
k_s	molecular diffusivity (salt)	1.1×10^{-9} m^2 s^{-1}
C_{pa}	specific heat of air	1004 J K^{-1} kg^{-1}
C_{po}	specific heat of water	3990 J K^{-1} kg^{-1}
α_s	surface albedo (ocean)	0.10
α_i	surface albedo (ice)	0.64
α_{sn-w}	surface albedo (wet snow)	0.73
α_{sn-d}	surface albedo (dry snow)	0.82
ϵ	surface emissivity	0.97
S_c	Solar constant	1353 W m^{-2}
σ	Stephan-Boltzmann constant	5.67×10^{-8} W m^{-2} K^{-4}
C_{HO}	transfer coefficient (ocean-air)	1.5×10^{-3}
C_{HI}	transfer coefficient (ice-air)	$2.0\times C_{HO}$
ν	viscosity	1.8×10^{-6} m^2 s^{-1}

magnitude of the fluxes of heat and salt from the modified UCDW to the base of AASW was first investigated using a simple box model [Smith et al., 1999] which indicated that double diffusion may play an important role in the vertical transfer of heat (primarily) and salt (slightly). In many high latitude systems where cold, fresh water overlies warm, salty water, double diffusion enhances the vertical transfer of heat and salt. The double diffusive instability results when the temperature contribution to the density profile is unstable but static stability is provided by the vertical distribution of salinity [Turner, 1973].

Indicators of the potential importance of the double diffusive instability are the density ratio (R_ρ) and its related diagnostic, the Turner angle (Tu).

$$\begin{aligned} R_\rho &= \beta S_z \cdot (\alpha T_z)^{-1} \\ Tu &= \frac{180^\circ}{\pi}\, tan^{-1}\left(\frac{1+R_\rho}{1-R_\rho}\right) \end{aligned} \tag{13}$$

where T_z (°C m^{-1}) and S_z (psu m^{-1}) are the vertical derivative of temperature and salinity, respectively and α (°C^{-1}) and β (psu^{-1}) are the thermal expansion and haline contraction coefficients, respectively. These two diagnostics measure the relative importance of the stabilizing effect of salinity to the destabilizing effect of temperature.

Values of $R_\rho > 1$ (and $Tu <$ -45°) indicate that conditions in the region favor the double diffusive instability and increased vertical fluxes of heat and salt are expected [Kelly, 1984]. For oceanic temperatures and salinities sampled on the shelf along the west Antarctic Peninsula shelf, the coefficient of haline contraction about 15 times that of thermal expansion (i.e. $\frac{\beta}{\alpha} \sim 15$). Given typical temperature and salinity differences across the 100 m thick pycnocline of 3.5°C (0.035 °C m^{-1}) and 0.5 (.005 psu m^{-1}), respectively, a typical density ratio for the region is 2.5 ($Tu \sim$ -65°).

With the potential for double diffusion established by R$_\rho$ > 1, several models exist to estimate the associated transfer of heat and salt. These models are based on laboratory observations [Turner 1973] that the heat transfer across a double diffusive interface is proportional to the temperature difference raised to the four-thirds power ($\Delta T^{\frac{4}{3}}$). A common $\Delta T^{\frac{4}{3}}$ model, proposed by Marmorino and Caldwell [1976] (MC76), estimates vertical fluxes of heat (Q_{dd}) across a double diffusive interface with the following empirical relationship

$$\begin{aligned} Q_{dd} &= 0.00859\, \rho_o\, C_{po}\, \alpha^{-1} \cdot (g\, k_t^2\, \nu^{-1})^{\frac{1}{3}} \\ &\quad \cdot exp\{4.6\, exp[-0.54 \cdot (R_\rho - 1)]\} \cdot (\alpha \Delta T)^{\frac{4}{3}} \end{aligned} \tag{14}$$

where ρ_o is the mean density, C_{po} is the specific heat of water, k_t is the molecular diffusivity for heat and g is the acceleration due to gravity (Table 2). A comparison of the MC76 to several other ($\Delta T^{\frac{4}{3}}$) models and a review of the double diffusive process are presented in Robertson et al. [1995].

It is convenient to express the double diffusive heat flux calculated by (14) in terms of its related mixing coefficient (K^T_{dd}). The double diffusive mixing coefficient can be found by solving

$$K^T_{dd} = Q_{dd}\left(\rho_o\ C_{po}\frac{\partial T}{\partial z}\right)^{-1} \tag{15}$$

A mixing coefficient for salt can be found using a relationship from Large, McWilliams and Doney (LMD) [Large et al., 1994] as follows

$$K^S_{dd} = \begin{cases} (1.85 - 0.85R_\rho)\ K^T_{dd}R_\rho^{-1} & \text{when} \quad 1 > R_\rho > 2 \\ 0.15\ K^T_{dd}R_\rho^{-1} & \text{when} \quad R_\rho > 2, \end{cases} \tag{16}$$

and is illustrated in Figure 10.

For typical pycnocline temperature and salinity values along the west Antarctic Peninsula, (14) gives a double diffusive heat flux (Q_{dd}) of about 10 W m^{-2}, which equates to a mixing coefficient (K^h_{dd}) of 5×10^{-5} m^2 s^{-1}. For density ratios characteristic of the west Antarctic Peninsula shelf waters, the typical mixing coefficient for salinity is significantly smaller than that for heat (i.e. $K^s_{dd} \sim 3\times10^{-6}$ m^2 s^{-1} for $R_\rho = 2.5$), a result typical of the double diffusive instability.

Given the potential importance of the double diffusive process along the west Antarctic Peninsula, its heat and salt transfer through the pycnocline will be considered when calculating ice-free heat budgets. The process will also be included in the modeling study. A full double diffusive heat flux calculation is presented in Section 4.1.3 for the 600.120 station.

3.3 Thermodynamic ice-ocean model

The thermodynamic ice-ocean model developed for this study is used to examine the role of vertical heat and salt fluxes on the seasonal evolution of the mixed

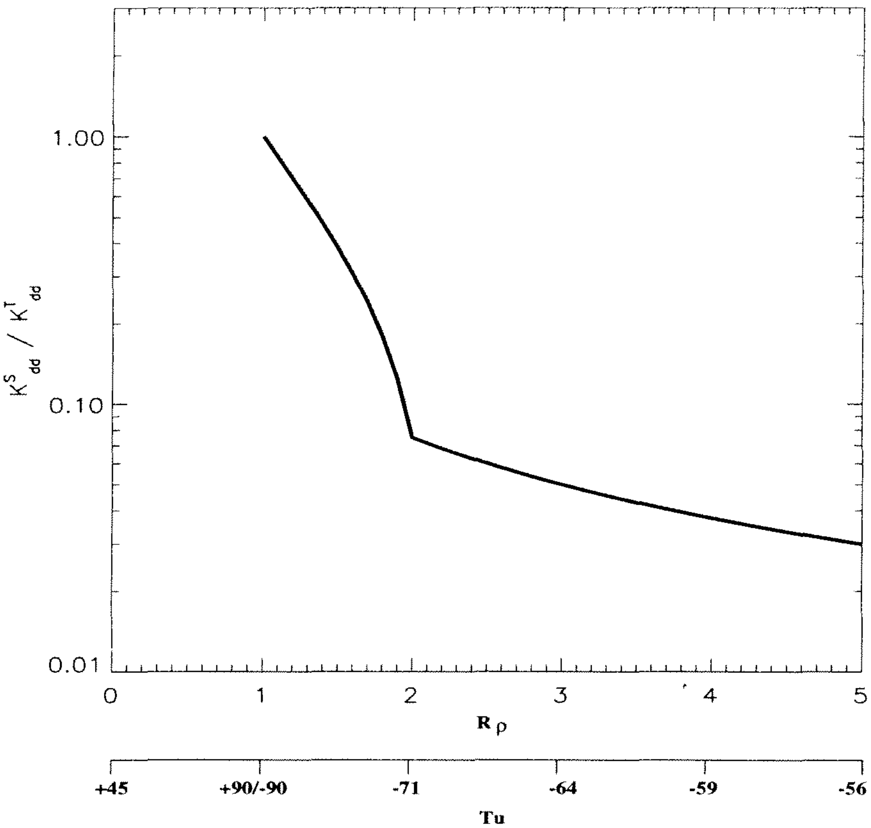

Figure 10. Double diffusive mixing coefficient K^S_{dd} (salt), normalized by K^T_{dd} (heat), as a function of the density ratio. Tu is indicated along the x-axis. For density ratios typical of those calculated for the shelf to the west of the Antarctic Peninsula (i.e. $R_\rho \sim 2$ to 2.5), $K^S_{dd} < 0.10\ K^T_{dd}$.

layer. In particular, the model will calculate the density structure of AASW as it reacts to surface fluxes of heat and salt, which are calculated as discussed in the previous section. A description of the equations of motion and the equations for oceanic temperature and salinity are presented in Section 3.3.1 while the ice model is described in Section 3.4. Numerical details such as vertical grid spacing, time stepping and numerical solution techniques are discussed in Section 3.5 for the entire ice-ocean model.

3.3.1 Ocean model equations

The ocean model is based on the vertical portion of the Princeton Ocean Model (POM) [Mellor, 1993; and Blumberg and Mellor, 1987], which includes prognostic equations for current velocity, temperature, and salinity. The Mellor-Yamada level 2.5 turbulence closure scheme (MY2.5) provides time dependent vertical mixing coefficient for momentum and scalar properties (K_m and K_h), respectively.

The governing equations for horizontal momentum (u,v) are

$$\frac{\partial(u,v)}{\partial t} = f(v,-u) + \frac{\partial}{\partial z}\left[(K_m + K_m^{Ri_g})\,\frac{\partial(u,v)}{\partial z} \right] \tag{17}$$

where K_m is the time-dependent, turbulent mixing coefficient for momentum from the MY2.5 turbulence scheme, and $K_m^{Ri_g}$ is a gradient Richardson number parameterization of mixing resulting from shear instabilities. This last process is an enhancement to the standard mixing scheme of POM and is described in Section 3.3.2.

The equations for time and vertical temperature (T) and salinity (S) structure are:

$$\frac{\partial T}{\partial t} = \frac{\partial}{\partial z}\left[(K_h + K_h^{Ri_g} + K_{dd}^T)\,\frac{\partial T}{\partial z} \right] + F_T^{nudge} \tag{18}$$

$$\frac{\partial S}{\partial t} = \frac{\partial}{\partial z}\left[(K_h + K_h^{Ri_g} + K_{dd}^S)\,\frac{\partial S}{\partial z} \right] + F_S^{nudge} \tag{19}$$

where K_h and $K_h^{Ri_g}$ are the MY2.5 turbulent, and gradient Richardson, mixing coefficients, respectively, for heat and salt. The differential transfer of heat and salt through the permanent pycnocline by double diffusion (Section 3.2) may be important along the west Antarctic Peninsula shelf, so this process is parameterized in the model by K_{dd}^T and K_{dd}^S (details are presented in Section 3.3.4). Given the vertical representation of the ocean model used in this study, (18) and (19) do not directly include the process of upwelling on the distribution of temperature and salinity. Such a process would have to be directly imposed or assumed to be part of the background diffusion. However, there is no significant lifting observed in the across-shelf density structure [Hofmann and Klinck, 1998; Smith et al., 1999] which would indicate that persistent upwelling is occurring in the region. Thus, the process of upwelling is not directly included in the model.

The last terms in (18) and (19) allow the simulated temperature and salinity to be forced back to a specified climatology. These terms prevent drift in the hydrographic structure of the sub-pycnocline waters which would occur in the absence of horizontal processes. This relaxation scheme and the relaxation time used is explained in Section (3.3.5).

3.3.2 Level 2.5 turbulence closure scheme

Full details on the MY2.5 turbulence closure scheme are presented in Mellor and Yamada [1974]. A brief overview is presented here as a reference.

The MY2.5 turbulence scheme provides time and space dependent turbulent mixing coefficients for momentum and scalar properties such as temperature and salt (K_m and K_h, respectively) by equating $(K_m, K_h) = ql(S_m, S_h)$, where S_m and S_h are derived stability factors and are geometrically determined from properties in the fluid (e.g., vertical momentum and density structures). The MY2.5 scheme requires tracking two additional prognostic variables: twice the kinetic energy (q^2) and the turbulence macroscale (l). Equations similar in form to (18) and (19) (without the enhancements from double diffusion and gradient Richardson mixing) are used to solve for q^2 and l.

3.3.3 Gradient Richardson mixing

A deficiency of all turbulence closure schemes is their inability to realistically represent mixing in highly stratified conditions [Large et al., 1994; Kantha and Clayson, 1994]. This problem is significant in conditions with melting ice, which introduces a very thin layer of fresh water which then warms with surface heating, and stabilizes the top of the water column.

Kantha and Clayson [1994] include a mixing scheme which parameterizes shear induced instabilities and the breaking of internal waves in an attempt to remove limitations of the MY2.5 scheme. This scheme depends on the gradient Richardson number,

$$Ri_g = N^2 \left(\left(\frac{\partial u}{\partial z} \right)^2 + \left(\frac{\partial v}{\partial z} \right)^2 \right)^{-1} \tag{20}$$

where N is the buoyancy frequency (rad s^{-1}) and u and v are the horizontal components of velocity. The scheme calculates $K_m^{Ri_g}$ based on the gradient Richardson number as follows

$$K_m^{Ri_g} = \begin{cases} \alpha_b & \text{when } Ri_g > Ri_c \\ \alpha_b + 5 \times 10^{-3} \cdot \left[1 - \left(\frac{Ri_g}{Ri_c}\right)^2\right]^3 & \text{when } 0 < Ri_g < Ri_c \\ \alpha_b + 5 \times 10^{-3} & \text{when } Ri_g < 0, \end{cases} \tag{21}$$

where α_b is a constant background diffusivity and is set to 10^{-5} m^2 s^{-1} for momentum and 10^{-6} m^2 s^{-1} for temperature and salinity [Kantha and Clayson, 1994].

As in the Kantha and Clayson [1994] study, Ri_c=0.7 is defined as the critical Richardson number. At Richardson numbers greater than the critical value, $K_m^{Ri_g}$ reduces to a constant background diffusivity (α_b) used in the standard POM mixing scheme. Richardson mixing coefficients for scalar properties ($K_h^{Ri_g}$) in (18) and

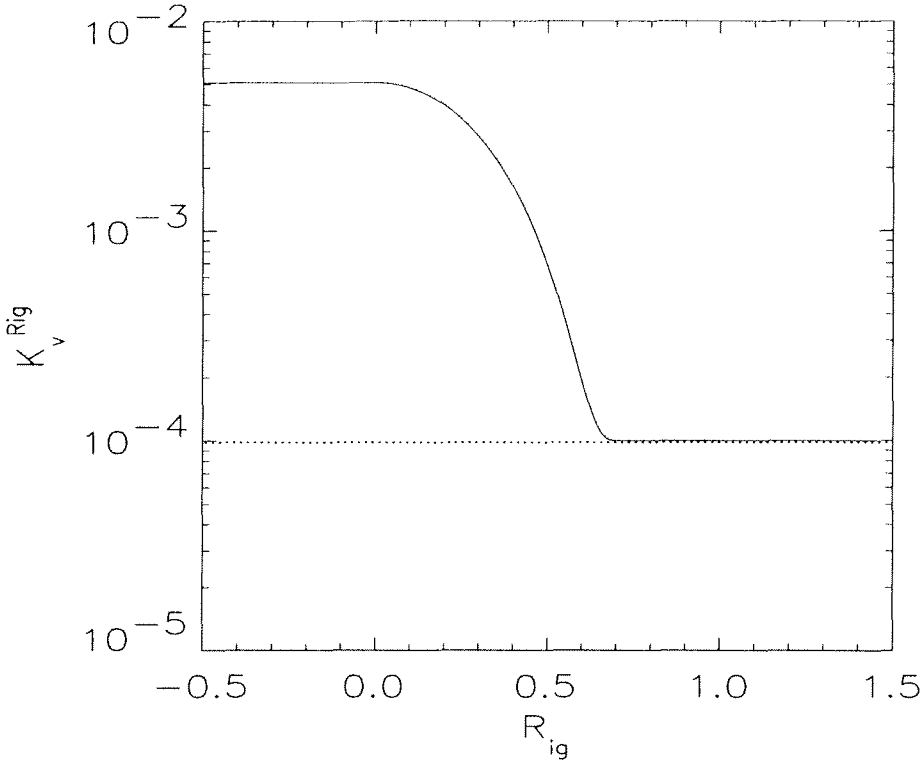

Figure 11. The gradient Richardson mixing coefficient (m^2 s^{-1}) as a function of the Richardson number. The figure is presented for a background diffusivity of 10^{-4} m^2 s^{-1} (dotted line).

(19) are found using the same formulation with different choices for the background diffusivity. The vertical mixing coefficient for momentum as a function of Richardson number is presented in Figure 11 where the default back to background mixing at Richardson numbers greater that 0.7 is indicated with a horizontal dotted line.

3.3.4 Double diffusive mixing

Double diffusive fluxes of heat and salt are calculated with the $\Delta T^{\frac{4}{3}}$ model of Marmorino and Caldwell [1976] (details presented in Section 3.2). Numerically, vertical profiles of the density ratio (R_ρ) are calculated from profiles of temperature and salinity at every time step. In regions of the water column where the density ratio is greater than 1, a double diffusive heat flux (Q_{dd}) is calculated from (14). Mixing coefficients for heat and salt are calculated using (15) and (16) and added to the standard mixing scheme given by (18) and (19).

3.3.5 Data nudging for temperature and salinity

Calculations presented in Klinck [1998] and in Smith et al., [1999] indicate the importance of lateral fluxes of heat and salt (summarized in Figure 2). Given that the model is vertical and time dependent, a source term must be added to (18) and (19) to artificially represent this lateral exchange. Thus, nudging terms are added to the governing equations as a source (or sink) of heat and salt for the sub-pycnocline waters.

The nudging term for temperature in (18) is implemented as

$$F_T^{nudge} = \nu(z) \cdot (T' - T) \tag{22}$$

where the model (T) is driven to some specified climatology (T'). The depth dependent nudging parameter ($\nu(z)$) can have values within the range of 0 (no nudging) to Δt^{-1} (full data replacement). A similar expression is used for salinity nudge in equation (19).

For all simulations presented in this study, $\nu(z) = \Delta t^{-1}$ at depth so that the sub-pycnocline temperature and salinity are replaced with the climatology (Figure 12a) at every time step. The strict nudging implemented in the sub-pycnocline waters is relaxed through the permanent pycnocline to zero in the top 200 m (Figure 12b) where the model is designed to track the complex density structure of AASW as it reacts to forcing at the air-ice-sea interface.

While the model is configured to allow nudging to any specified temperature or salinity, the initial conditions used in this model represent the climatology in the model (Figure 12a). The initial conditions for AASW are obtained by averaging all of the hydrographic profiles from stations occupied during the 1993 winter cruise. Initial conditions for the sub-pycnocline waters are obtained by averaging the profiles from all four cruises. Comparing the results of this calculation to those presented in Hofmann et al. [1996] indicates that the sub-pycnocline averages represent climatology for the west Antarctic Peninsula shelf waters.

Methods other than nudging could have been used to keep the sub-pycnocline waters from drifting. An alternative technique is to hold the temperature and salinity of the bottom grid point constant, which assumes an infinite supply of deep water with the specified hydrographic properties. However, this approach forces heat and salt through the bottom only and fails to reproduce the structure of the sub-pycnocline waters. The method used in this study is designed to mimic horizontal fluxes of heat and salt between the UCDW and the modified UCDW (Qh in Figure 2) and maintains the structure of the sub-pycnocline waters without affecting AASW. It also allows the sub-pycnocline heat and salt fluxes to be calculated so that the lateral exchanges can be estimated.

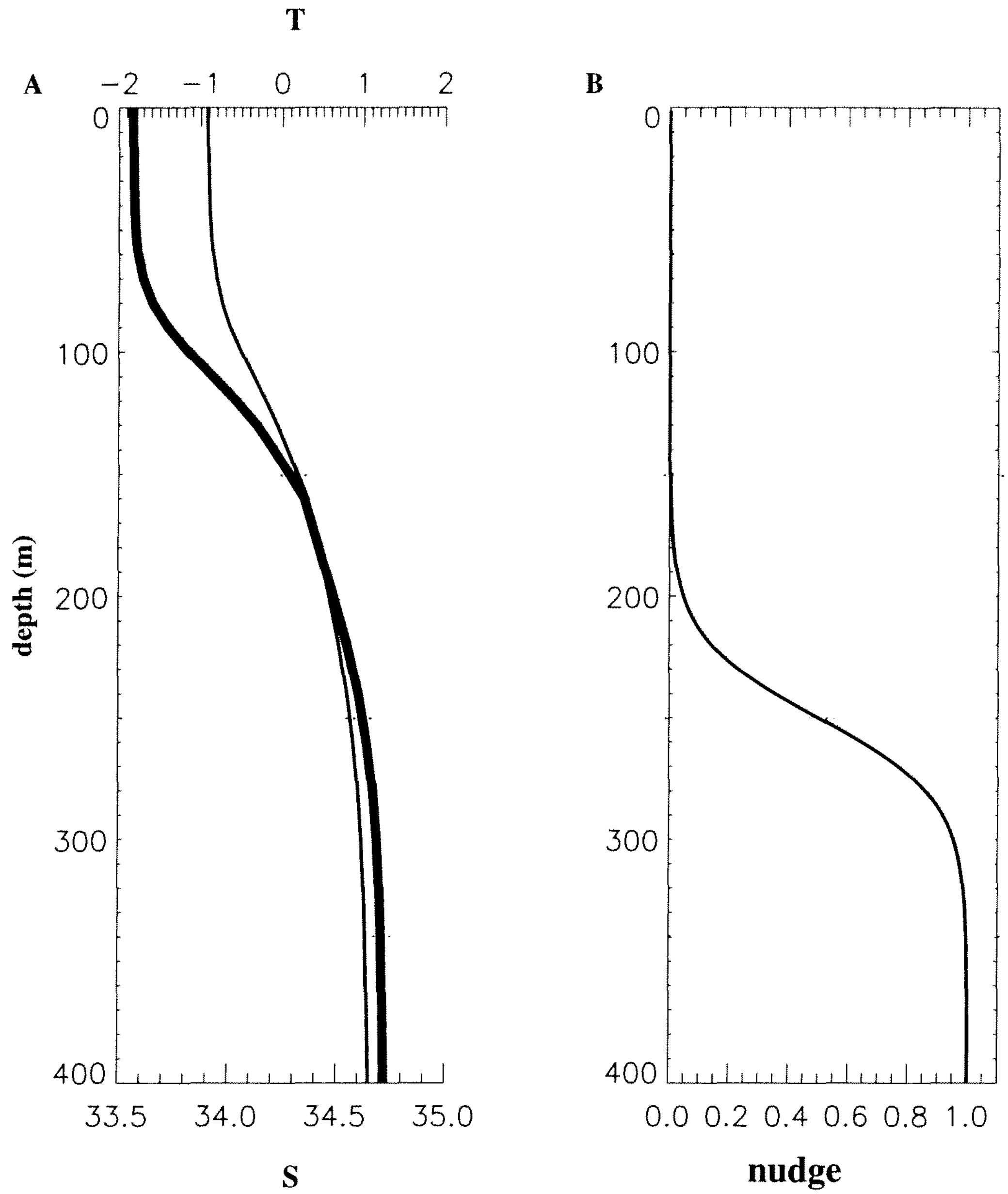

Figure 12. Nudging and climatology for the ice-ocean model. A) Vertical temperature (thick) and salinity (thin) profiles used for initial conditions and nudging. (B) Depth-dependent nudging parameter normalized by Δt. For $\nu(\Delta t)^{-1} = 0$ there is no nudging; for $\nu(\Delta t)^{-1} = 1$ the climatology replaces the simulated values.

3.4 Ice model

The sea ice model used in this study is based on a model presented in Mellor and Kantha [1989], Kantha and Mellor [1989] and Häkkinen and Mellor [1990]. This series of papers and the model itself will be referred to as the MKH papers and model.

The primary difference between the model used here and the MKH model is the treatment of thermodynamics within the sea ice. The MKH model includes one internal ice temperature point (i.e. Semtner 1-level ice model) while the model presented here follows the thermodynamics of the Semtner 0-level ice model [Semtner, 1976], which treats the ice as a uniform layer with thickness (h_i) and neglects internal ice thermodynamics. Effects of a temperature distribution within the ice are considered to be negligible for relatively thin ice (e.g., $h_i \sim 0.5$ to 1 m at maximum winter extent) as observed along the western Antarctic Peninsula.

The model (Figure 13) tracks four prognostic variables: area-averaged ice thickness ($h_i^{av} = A_i h_i$), percent local ice concentration (A_i) and the horizontal components of ice velocity (U_i and V_i). Changes in the ice thickness result from growth/melt rates at the air-ice, air-ocean and ice-ocean interfaces, which are produced by imbalances in the local heat fluxes.

3.4.1 Ice thickness and concentration

The equations for the area-averaged ice thickness and local ice concentration are given by

$$\frac{\partial \left(A_i h_i\right)}{\partial t} = \frac{\rho_o}{\rho_i}\left[A_i(Wio - Wai) + (1 - A_i)\left(Wao + Wfr\right)\right] \tag{23}$$

and

$$h_i \frac{\partial A_i}{\partial t} = \frac{\rho_o}{\rho_i}\left[\Phi(1 - A_i)Wao + \Psi A_i Wio + (1 - A_i)Wfr\right] \tag{24}$$

where the growth rates (m s^{-1}) associated with the air-ice, ice-ocean and air-ocean

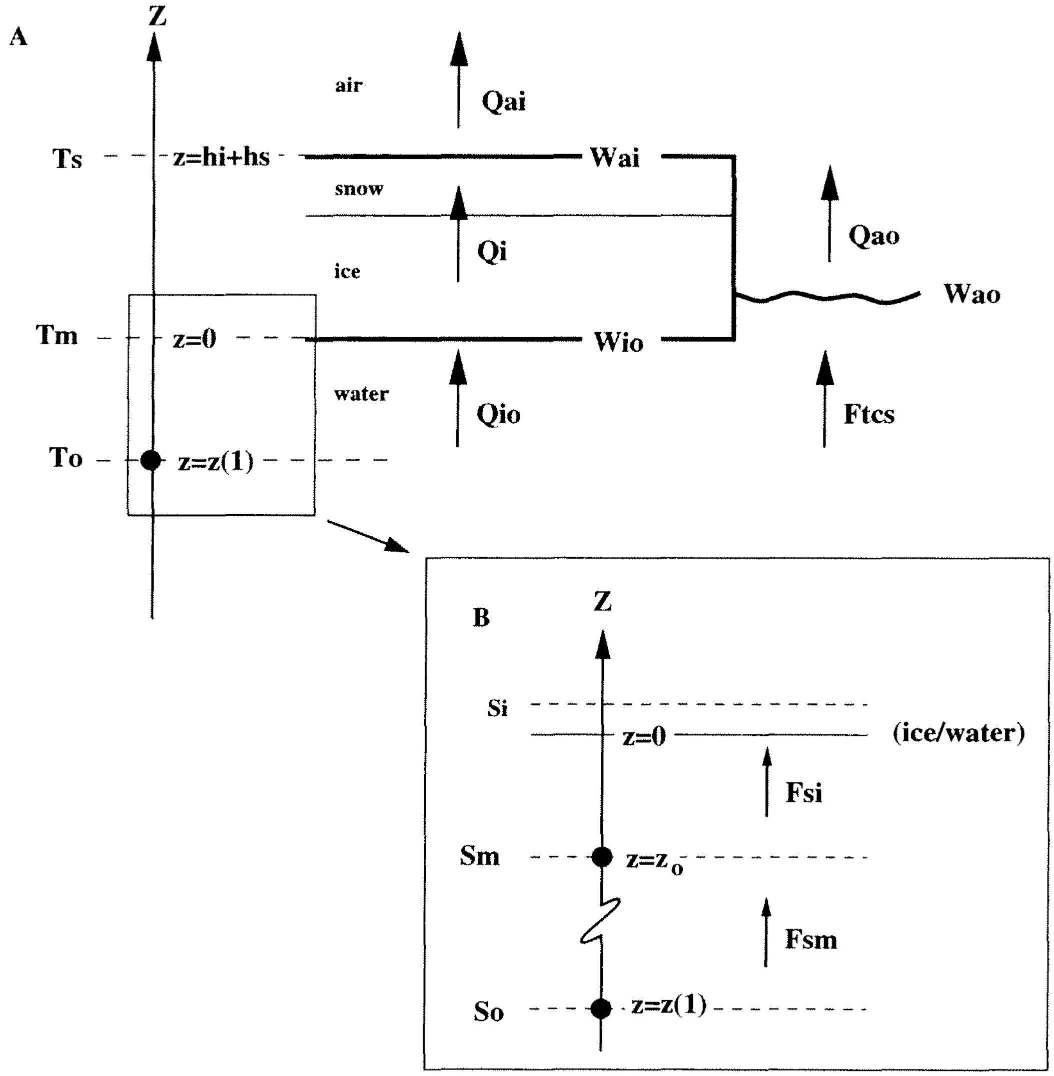

Figure 13. A schematic of the thermodynamics at the air-ice-ocean interface (with an optional, prescribed snow layer). A) Illustrated along the z-axis are the relative locations of the temperature at the ice-snow surface (*Ts*), base of the ice (i.e. molecular sub-layer) (*Tm*) and the first internal ocean grid point (*To*). The fluxes of heat from the ocean to the ice (*Qio*), the surface of the ice and open ocean to the atmosphere (*Qai* and *Qao*, respectively), through the ice (*Qice*) and from the internal ocean to the ocean surface (F_{tcs}) are indicated. Growth rates at the air-ice, (*Wai*), the ice-ocean (*Wio*) and open ocean (*Wao*) are indicated. B) An expanded schematic of the ice-water interface to illustrate salt fluxes from the molecular sub-layer to the ice (*Fsi*) and from the ocean to the molecular sub-layer (*Fsm*).

interfaces are indicated as Wai, Wio and Wao, respectively (Figure 13). Changes in ice thicknesses and concentration from horizontal ice motion (e.g., ice convergence and rheology) are neglected in this study. A convergence term can be added to (23) and (24), as in the MKH model; however, MKH specify the convergence term from observations in the Arctic ocean. Such observations do not exist for the west Antarctic Peninsula shelf region so the term is not included. The last term on the right hand side of (23) represents a growth rate associated with the conversion of sea water to frazil ice which occurs when the water column becomes super cooled (details in Mellor and Kantha [1989]). Frazil ice formation is calculated as part of the molecular sub-layer (Section 3.4.5); however, it was not found to play a significant role in ice production in the west Antarctic Peninsula region.

The process represented by (23) is the conservation of volume while (24) is an empirical relationship which merely partitions the thermodynamics from (23) into changes in ice thickness and concentration with the latter process interpreted as the opening and closing of leads. The parameters Φ and Ψ in (24) are tuning parameters and the values given in Häkkinen and Mellor [1990] are used,

$$\Phi = \begin{cases} 4.0 & \text{when} \quad Wao > 0 \text{ (growth)} \\ 0.0 & \text{when} \quad Wao < 0 \text{ (melt)} \end{cases}$$

$$\Psi = \begin{cases} 0.7 & \text{when} \quad Wio < 0 \text{ (melt)} \\ 0.0 & \text{when} \quad Wio > 0 \text{ (growth)} \end{cases} \tag{25}$$

where Φ and Ψ partition sea ice growth rates at the open ocean and under the ice.

The physical interpretation of the tuning parameters are as follows: for $A_i <$ 1% and Φ=1, Wao builds ice along the edges of leads thus preserving the thickness. Choosing the parameter to be greater than 1 is non-physical, but allows Wao to affect ice thickness as well as the concentration (MKH demonstrated the model is not sensitive to changes in this parameter once $\Phi > 2$). The Ψ term represents a reduction in ice concentration resulting from the differential removal of ice near leads [Häkkinen and Mellor, 1990].

3.4.2 Model heat fluxes

The total simulated heat flux is determined by combining ice-free, open ocean heat flux (Q_{ao}) calculated similarly as the ice-free, open ocean heat flux in Section 3.2 with through ice heat fluxes (Q_{ice}) calculated at every time step within the model. Meteorological variables of air temperature, relative humidity, cloud cover and atmospheric pressure obtained from the Faraday data set (Section 3.1.2) are used to calculate the surface fluxes of heat. The simulations also require sea surface temperature which is obtained from the top model grid cell. The oceanic heat flux (F_{tcs} in Figure 13b) is determined from the MY2.5 turbulence closure scheme using the top two oceanic grid points as:

$$F_{tcs} = \left(K_h + K_h^{Ri_g}\right) \frac{\partial T}{\partial z} \quad as\ z \rightarrow 0 \tag{26}$$

The double diffusive contribution near the sea surface is assumed to be negligible and is not included in (26).

The heat flux through the ice ($Qice$) is given by

$$Qice = \frac{k_s(T_s - T_m)}{h_s + \left(\frac{h_i \cdot k_s}{k_i}\right)} \tag{27}$$

where h_i and h_s are the thicknesses (m) of the ice and optional snow layers, respectively. The thermal conductivity of ice and snow are represented by k_i and k_s and T_m is the temperature at base of the ice in the molecular sublayer. Parameterizing the thermodynamic effects of the molecular sublayer [Mellor and Kantha, 1989; Steel et al., 1989] provides the thermodynamics coupling (Qio) between the ice and the ocean model (Section 3.4.5).

The air-ice heat flux (Qai) is calculated in a manner similar to the open ocean (Section 3.2), with sea surface temperatures (T_{sst}) and heat transfer coefficients (C_{HO}) in (11) and (12) replaced by the surface temperature of the ice (T_{ice}) and heat transfer coefficients appropriate for the air-ice interface. Choices for the transfer coefficient for ice (C_{HI}) and for surface albedos (Table 2) are consistent with choices in the MKH model and those in Ikeda [1989].

3.4.3 Ice growth rates

The surface temperature of the ice, T_s, is advanced from the current time level ($t = n$) to the next time level ($t = n + 1$) by

$$T_s^{n+1} = min \;\; (T_s^n + \Delta T_s, \; T_{melt}) \tag{28}$$

where T_s is always less than or equal to the melting point of ice (T_{melt}) which is a function of the salinity within the ice (S_i) defined in Fujino [1974] as

$$T_{melt} = -m \cdot S_i - n \cdot z \tag{29}$$

where m and n are defined to be 5.43×10^{-2} K psu^{-1} and 7.59×10^{-4} K m^{-1}, respectively. Ice salinity is held constant throughout the simulations and is prescribed to be 8. Similar studies use various values for the salinity of sea ice with thick Arctic ice having values order of 4 to 5 [Häkkinen and Mellor, 1990; Parkinson and Washington, 1979] while thinner ice of Marginal Ice Zones (MIZ) have been characterized with salinities as high as 8 to 10 [Kamph and Backhaus, 1998].

The temperature change at the ice surface (ΔT_s) is obtained by assuming a balance of the heat flux at the air-ice interface balances (i.e. Qai=$Qice$). Using (28), the change must satisfy

$$\begin{aligned} \frac{k_s(T^n + \Delta T_s - T_m)}{h_s + \left(\frac{h_i \cdot k_s}{k_i}\right)} \;=\; Q_{solar}^{ice} \;\; &+ \;\; \epsilon\sigma \cdot (T^n + \Delta T_s + 273)^4 \;\; + \\ &\rho_a C_{pa} C_{HI} W \left(T^n + \Delta T_s - T_{air}\right) \end{aligned} \tag{30}$$

where Q_{solar}^{ice} is the combined affects of Q_{sw}, Q_{lw}^{down} and Q_{lat} over the ice. Solving (30) for (ΔT_s) yields an implicit equation for the temperature change (recall that

Q_{ice}^{solar} depends on T_s) which can be iterated to obtain the ice temperature change, and the new T_s. This calculation usually converges within 2 to 3 iterations.

Once the new T_s is found, heat fluxes are calculated. Any imbalance between through ice heat fluxes and those at the atmosphere-ice interface from setting surface temperatures to the freezing point results in surface melting. The fresh water flux from this surface melting is immediately added to the water column through the leads (i.e. no melt ponds are allowed to form). The surface melting is calculated as

$$Wai = \frac{(Qai - Qice)}{\rho_o L_f} \tag{31}$$

where L_f is the latent heat of fusion (Table 2). Note that iterating on ΔT such that $Qice = Qai$ forces the growth rate at the atmosphere-ice interface to be zero under non-melting conditions as the numerator in (31) vanishes. This makes physical sense because there is no water at the atmosphere-ice interface to form ice.

Similarly, growth rates at the base of the ice and at the atmosphere-ocean interface are calculated from imbalances in respective heat fluxes as (details in Section 3.4.5),

$$Wio = \frac{(Qice - Qio)}{\rho_o L_f} \tag{32}$$

$$Wao = \frac{(Qao - F_{tcs})}{\rho_o L_f} \tag{33}$$

The growth rate at the base of the ice can be positive (ice growth) or negative (ice melt) depending on the relative magnitudes of the fluxes. Growth rates at the atmosphere-ocean interface are constrained to be positive (growth) or zero by the choices of Φ (25) which eliminates the possibility of melting at the sides of the leads. The thermodynamic effects of leads are included by allowing heat to warm the surface and which increases melting at ice-ocean interface.

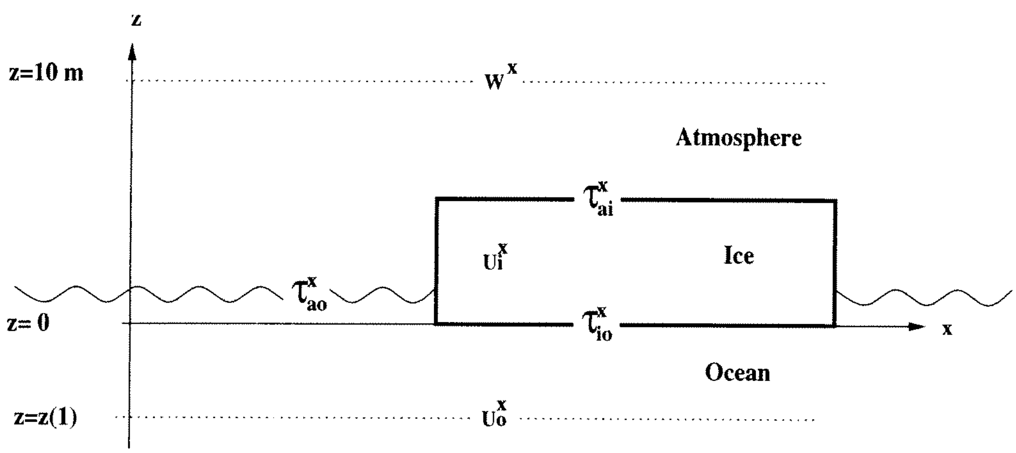

Figure 14. Schematic for the ice-ocean model interfacial stress terms ($\hat{x}$ direction). Illustrated along the z-axis are the relative locations of wind speed, (W^x), ice-snow velocity (U_i) and ocean velocity (U_o^x). Also indicated are the interfacial drag at the air-ice (τ_{ai}^x), ice-ocean (τ_{io}^x) and air-ocean (τ_{ao}^x) interfaces.

3.4.4 Ice momentum equations

The primary role of ice velocity in this model is to provide mixing to the ocean model under ice covered conditions. The ice slab is modeled as a free drifting block (e.g., no internal effects from rheology) forced by wind stress at the air-ice interface (τ_{ai}) and interfacial ice-water drag (τ_{io}). The free drift equations [Ikeda, 1989] are

$$A_i h_i \frac{\partial(U_i, V_i)}{\partial t} = A_i h_i f\ (V_i, -U_i) + \frac{A_i}{\rho_i} \cdot \left(\tau_{ai}^{(x,y)} - \tau_{iw}^{(x,y)}\right) \tag{34}$$

where ρ_i is the density of ice (Table 2) and the superscript x and y on τ_{ai} and τ_{iw} denote the component associated with U_i and V_i, respectively.

Simple drag laws are used to calculate the drag at the air-ocean and the open ocean, air-water (τ_{ao}) interfaces (Figure 14).

3.4.5 Ice-ocean model coupling and surface boundary conditions

The surface boundary condition used for the ocean model is [Mellor and Kantha, 1989],

$$\rho_o K_m \frac{\partial(u, v)}{\partial z} = A_i \tau_{io}^{(x,y)} + (1 - A_i)\, \tau_{ao}^{(x,y)} \tag{35}$$

where K_m is the mixing coefficient for momentum from the MY2.5 scheme (Section 3.3.2). The ice-ocean stress ($\tau_{io}^{(x,y)}$) is given by

$$\tau_{io}^{(x,y)} = \frac{\kappa\mu}{ln(\frac{z}{z_o})} \Delta(u, v) \tag{36}$$

where κ=0.4 is the von-Karman constant and $\mu = [(\tau_{io}^x)^2 + (\tau_{io}^y)^2]^{\frac{1}{4}} \cdot \rho_o^{-\frac{1}{2}}$ is the friction velocity. The roughness parameter (z_o) is calculated as in the MKH studies and $\Delta(u, v)$ is the velocity difference between the ice and the ocean defined at the top oceanic grid point. The interfacial stress calculated in this step forces both the ocean and ice models, thus providing momentum coupling between the two. Typical stress values as a function of wind speed for the 1993 simulation (Section

4.3.2) are indicated in Figure 15 and are consistent with those reported in Wamser and Martinson [1993] for the Weddell Sea.

The thermodynamic coupling between the ice and ocean models (as in the MKH model) is based on the parameterization of a molecular sub-layer [Steel et al., 1989], which is a thin layer at the base of the ice. The molecular sub-layer is assumed to be at the freezing temperature ($T_m = T_f(S_m)$) (Figure 13b). The numerical details for parameterizing the molecular sub-layer are presented in Mellor and Kantha [1989] but are summarized here.

The key equations for the thermodynamic coupling involve heat and salt fluxes between the ocean and the molecular sub-layer. These equations are

$$F_{T_{o\to m}} = -\rho_o C_{po} C_{T_z} (T_m - T_o) \tag{37}$$

$$F_{S_{o\to m}} = -C_{S_z} (S_m - S_o) \tag{38}$$

where S_o is the oceanic salinity, C_{T_z} and C_{S_z} are heat and salt exchange coefficients, respectively, and depend on molecular diffusivities as described in MKH and in Steel et al. [1989].

The salt flux between the molecular sub-layer and the ice is given by

$$F_{S_{m\to i}} = (S_i - S_o) \cdot [\ A_i \cdot (Wio - Wai) + (1 - A_i) \cdot Wao\ ] + S_o (P - E) \tag{39}$$

where $(P-E)$ is net precipitation over evaporation and the growth rates (Wai, Wio and Wao) are obtained from the current time level. Evaporation (E) is assumed to be zero while precipitation (P) prescribed from the atmospheric data (Section 3.1.2).

The daily averaged precipitation records from Palmer station are converted into an annual average of 2.07×10^{-8} m s^{-1} and added to the model at every time step. This annual average agrees well with Cullather et al. [1998] who obtain net precipitation on the order of 500 - 700 mm yr^{-1} (1.5 - 2.2×10^{-8} m s^{-1}) for the west

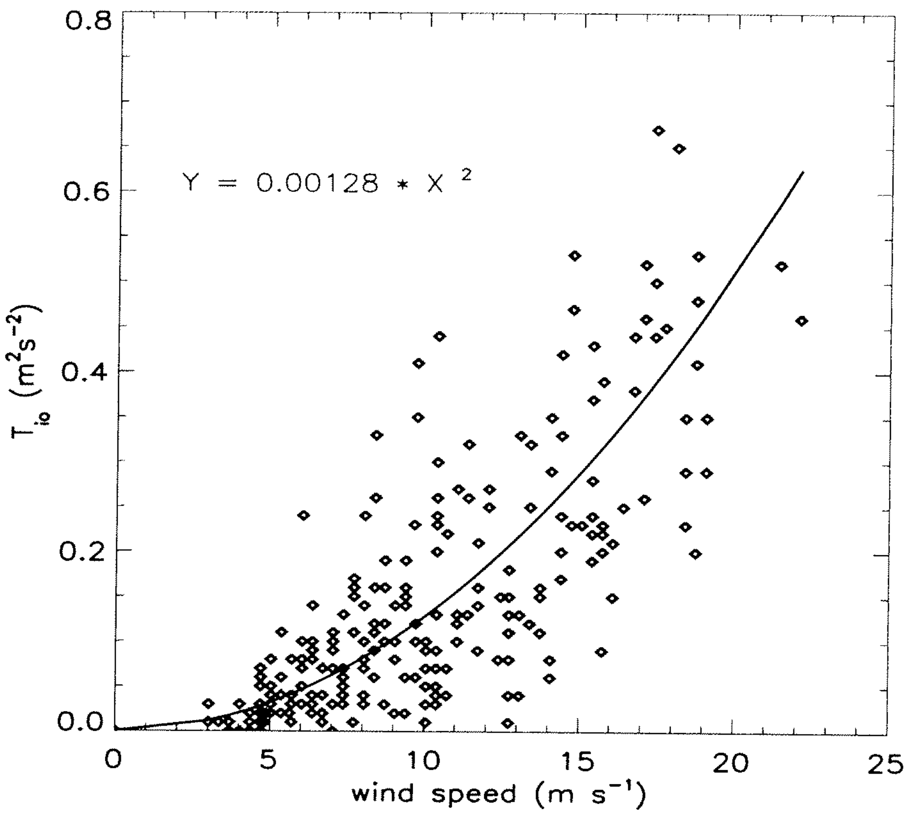

Figure 15. Ice-ocean stress as a function of wind speed. A least squares quadratic curve of best fit to the data is indicated with the solid curve.

Antarctic Peninsula region. The model accumulates snow if the surface temperature of the ice is colder than the freezing point, otherwise, the precipitation enters the ocean as water through open leads.

Salinity at the ice-ocean interface is found by equating (38) and (39). The melting point (T_m) is then obtained from local salinity (S_m) using (29) which is substituted into (37) and equated to the heat flux at the ice-ocean interface. Coupling between the models is achieved by forcing both models with these fluxes.

3.5 Numerical details

The ocean model is integrated in time using an implicit scheme described in Mellor [1993] and Blumberg and Mellor [1987]. The implicit scheme is designed for the full three-dimensional model and removes time stepping constraints from small values of vertical grid spacing and possible large values of vertical viscosities.

An Euler scheme is used to solve (23) and (24). The ice momentum equations (34) are a stiff set of equations with the potential for small oscillations in the forcing to be amplified by the inverse of ice thickness (i.e. h_i^{-1}). Because of this singularity, h_i is never allowed to go to zero. Instead it is held at a very small number ($h_{i_{min}} = 10^{-3}$ m) and A_i is allowed to vanish under conditions of no ice cover. For model stability, (34) is solved implicitly.

The time step (Δt) for all model simulations is 900 s (15 minutes) which is smaller than necessary for the simulations presented, but was chosen in anticipation of extending the model to three dimensions in the future. The model depth is 400 m and is resolved with 150 levels giving a vertical grid spacing (Δz) of 2.6 m. This vertical grid spacing was found to be smaller than needed, but resolved features in AASW such as vertical stratification. Further decreasing Δz did not improve the simulations but increased run time. Decreasing the vertical resolution decreased the ability to simulate features in the upper portion of AASW while producing no significant change in the pycnocline or sub-pycnocline portion of the model. This latter result is most likely produced by the relaxation scheme and would need to be re-examined if nudging to climatology was removed or modified.

CHAPTER 4
RESULTS

The first portion of this chapter presents results from a AASW heat budget constructed using atmospheric and oceanic data measured in 1993. The second portion presents results of the oceanic response and the dynamics of the mixed layer under the atmospheric forcing obtained with the time and vertically dependent, coupled sea ice-ocean model.

4.1 AASW heat budget for 1993

4.1.1 Atmospheric regime

The winds along the west Antarctic Peninsula are typically strong, exceeding 15 to 20 m s^{-1} (30 to 40 knots) and are predominantly onshore to the southwest, or towards the north or northeast (Figure 16a). Air temperatures recorded at Faraday Station for 1993 had summer maximum temperatures around 5°C and winter lows around -15°C (Figure 16b). These winter temperatures fall in the mid-range of winter lows when compared to other years (Figures 9a).

Atmospheric conditions along the shelf to the west of the Antarctic Peninsula are warm compared to conditions in the interior of Antarctica. They are warmer than temperatures recorded along other Antarctic coastal regions characterized by permanent ice cover (e.g., Weddell Sea) [Smith et al., 1996] and are an indication that the shelf west of the Antarctic Peninsula can be characterized by a maritime climate. Daily averaged relative humidities along the peninsula are in excess of 80% while cloud cover is typically 80 to 90% (Figures 16b,c); a further indication of the maritime climate which characterizes the west Antarctic Peninsula shelf region.

All 1993 atmospheric parameters recorded at Faraday show variability about weekly intervals within which are embedded shorter (2-to-4 day) fluctuations. These events occur approximately weekly and is associated with the passage of storms and their associated warm/cold fronts. Storm-scale variability occurs throughout the year (Figure 16), but the largest reversals are in the mid-winter temperature record which can increase from winter lows (-15°C) to summer-like temperatures (0°C) in one day and remain there for 5-10 days.

The wind record at Faraday can be used to partition the atmospheric regime into two general categories: strong, warm winds blowing down the coast, and weaker, cold winds blowing onshore from the west or south (Figures 16a,b and 17). The mid-winter temperature reversals are related to reversals in the wind field with warmer atmospheric conditions prevailing when winds are from the north. The relationship between the winds and the air temperatures persists for the entire year, but is most pronounced during the winter and spring seasons (Figure 17).

Cumulative wind rosettes for the 1993 Faraday Station (Figures 17) represents conditions over the entire year. Winds along the west Antarctic Peninsula are predominantly from the northeast or southwest (Figure 17a). Winds from the northeast are associated with air temperatures which are 5°C warmer than times with winds from the south (Figure 17c). Seasonal relationships between wind direction, speed and air temperatures can be seen in Figure 17d-o.

Sea surface temperatures (SST) (Figure 16e) (Section 3.1.3) range from summer highs of 1.6°C to freezing conditions in the winter (T_f = -1.8 to -2.0°C for salinities $\sim$ 33.8 to 34.0).

The ice free period near Palmer Station (day 0 through 170) is followed by 5 to 6 months of ice cover (Figure 16f). At the time of maximum winter ice extent, the region is characterized by 80% ice cover. Ice develops around day 170 with a rapid advance lasting several weeks. The initial growth period is followed by alternate ice growth and retreat which persists from day 190 to the time of maximum winter ice extent around day 305-310. A rapid spring melt begins around day 290 and

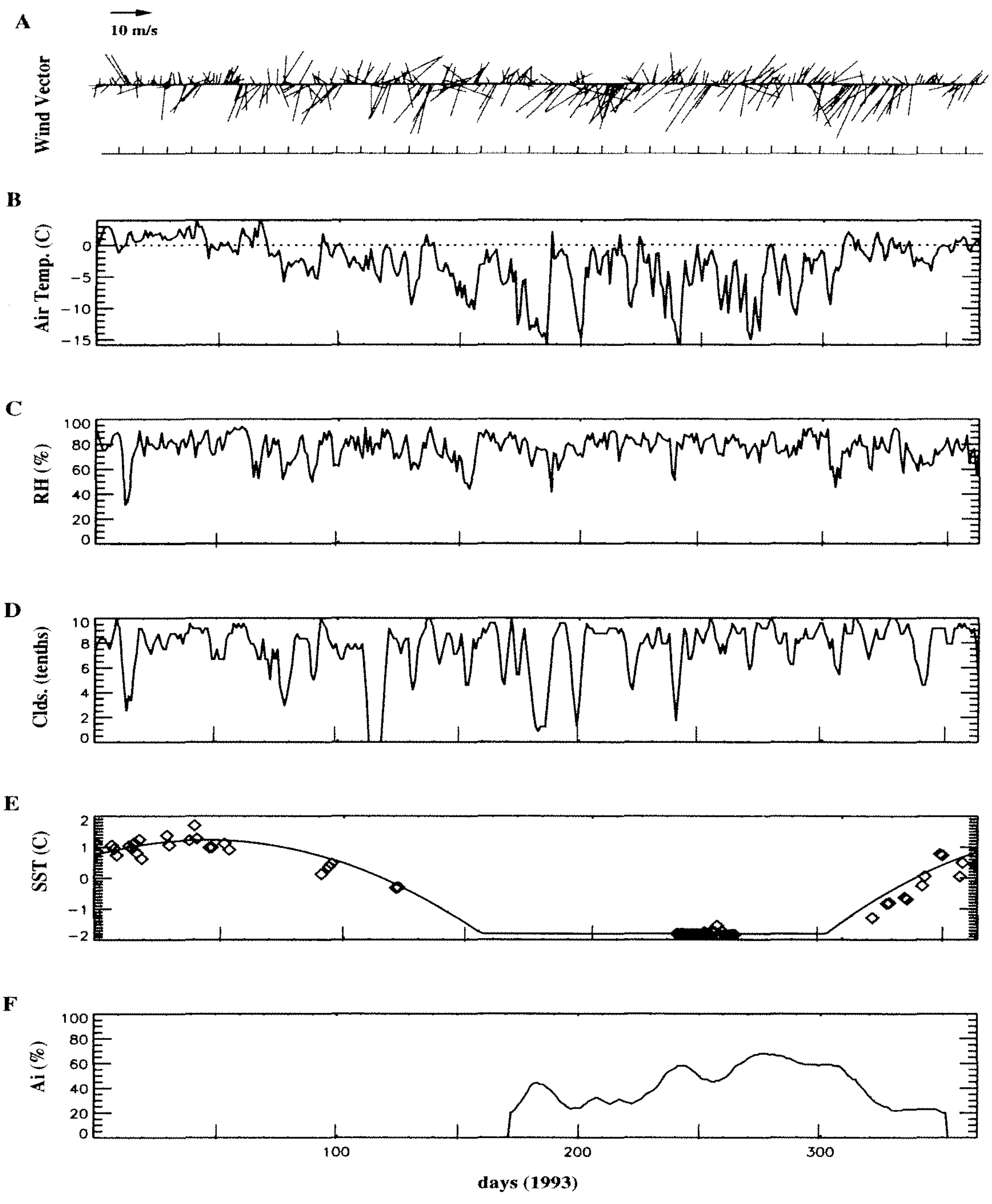

Figure 16. Atmospheric and oceanic variables for the 1993 ice free heat budget. Daily-averaged time series of A) Wind vectors (+ x-axis aligns with East), B) air temperature, C) relative humidity, D) cloud cover, E) near-Palmer SST (details in Section 3.1.3) and F) near-Palmer, ice concentrations. Observations are smoothed with a 7 day filter for presentation.

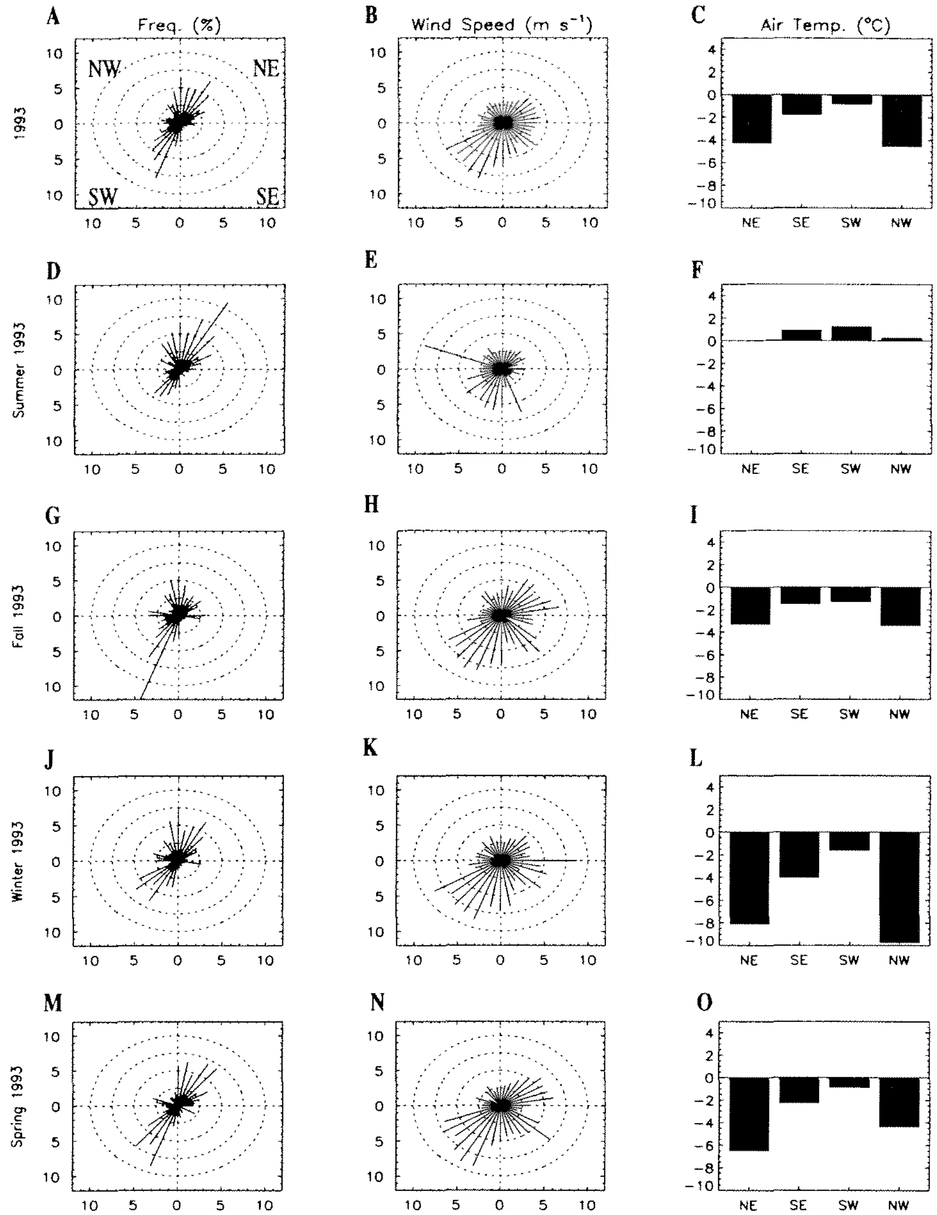

Figure 17. Cumulative 1993 wind rosettes for Faraday Station. A) The percentage of wind observations recorded at Faraday Station in a given 10° bin (NW, NE, SE and SW quadrants are labeled for reference). B) Average speed of all wind observations (m s^{-1}) blowing towards a given 10° bin. C) Average air temperature (°C) for winds blowing towards a given quadrant (i.e. winds blowing towards NE had an average wind speed below 5 m s^{-1} and corresponded to average temperatures of -5°C). Panels D to O provide the seasonal breakdown of A to C.

Table 3. Ice free heat flux statistics (W m^{-2}) for times consistent with three cruises to the west Antarctic Peninsula during the 1993 sampling season. All heat fluxes are rounded to the nearest 5 with positive fluxes indicating AASW warming (i.e. positive down).

LTER Cruise ID	Q_{open}	Q_{sw}	Q_{lw}	Q_{sens}	Q_{lat}
93A	110 $\pm$ 50	160 $\pm$ 70	-30 $\pm$ 15	5 $\pm$ 5	0 $\pm$ 5
93B	-90 $\pm$ 45	25 $\pm$ 15	-50 $\pm$ 20	-40 $\pm$ 30	-10 $\pm$ 5
93C	-30 $\pm$ 15	20 $\pm$ 5	-20 $\pm$ 10	-30 $\pm$ 25	-5 $\pm$ 5

continues through the spring until the ice vanishes. The initial spring melt is rapid but stalls around day 325 for several weeks.

4.1.2 Ice free, surface heat budget for surface waters

The atmospheric conditions presented in the previous section are used with the bulk aerodynamic equations presented in Section 3.2 to calculate a surface heat budget (Q_{open}) for the ice free shelf waters along the west Antarctic Peninsula (Figure 18). A summary of total budget and its individual terms over the times of the three 1993 cruises is presented in Table 3.

The short wave flux (Qsw) ranges from a summer maximum of 200 to 250 W m^{-2} to winter lows near 0 W m^{-2} (Figure 18a). From day 0 to 100, and again from day 300 to 365 (i.e. fall and summer months), short wave radiation is the dominant term in the surface heat budget providing nearly all of the heating (Figure 18a,c). Net long wave radiation (Q_{lw}^{down}-Q_{lw}^{back}) is a persistent oceanic loss with an annual average of 30 W m^{-2} and times when the losses are 80 W m^{-2}. This term becomes important in the overall heat budget during the fall when the dominance of short wave radiation diminishes sufficiently that long wave radiation cancels its heating effects. Short and long wave radiation balance around day 70 when SST begins to fall (Figure 16e).

From late-spring to early-fall, the ocean-atmospheric temperature difference is